



## Development of iminosugar-based glycosidase inhibitors as drug candidates for SARS-CoV-2 virus via molecular modelling and in vitro studies

Zorana Ferjancic, Filip Bihelovic, Bojan Vulovic, Radomir Matovic, Milena Trmcic, Aleksandar Jankovic, Milos Pavlovic, Filip Djurkovic, Radivoje Prodanovic, Aleksandra Djurdjevic Djelmas, Nevena Kalicanin, Mario Zlatovic, Dusan Sladic, Thomas Vallet, Marco Vignuzzi & Radomir N. Saicic

**To cite this article:** Zorana Ferjancic, Filip Bihelovic, Bojan Vulovic, Radomir Matovic, Milena Trmcic, Aleksandar Jankovic, Milos Pavlovic, Filip Djurkovic, Radivoje Prodanovic, Aleksandra Djurdjevic Djelmas, Nevena Kalicanin, Mario Zlatovic, Dusan Sladic, Thomas Vallet, Marco Vignuzzi & Radomir N. Saicic (2024) Development of iminosugar-based glycosidase inhibitors as drug candidates for SARS-CoV-2 virus via molecular modelling and in vitro studies, *Journal of Enzyme Inhibition and Medicinal Chemistry*, 39:1, 2289007, DOI: [10.1080/14756366.2023.2289007](https://doi.org/10.1080/14756366.2023.2289007)

**To link to this article:** <https://doi.org/10.1080/14756366.2023.2289007>



© 2023 The Author(s). Published by Informa UK Limited, trading as Taylor & Francis Group.



[View supplementary material](#)



Published online: 12 Dec 2023.



[Submit your article to this journal](#)



Article views: 1424



[View related articles](#)



[View Crossmark data](#)

RESEARCH ARTICLE



## Development of iminosugar-based glycosidase inhibitors as drug candidates for SARS-CoV-2 virus via molecular modelling and *in vitro* studies

Zorana Ferjancic<sup>a</sup>, Filip Bihelovic<sup>a</sup>, Bojan Vulovic<sup>a</sup>, Radomir Matovic<sup>c</sup>, Milena Trmcic<sup>b</sup>, Aleksandar Jankovic<sup>c</sup>, Milos Pavlovic<sup>a</sup>, Filip Djurkovic<sup>a</sup>, Radivoje Prodanovic<sup>a</sup>, Aleksandra Djurdjevic Djelmas<sup>a</sup>, Nevena Kalicanin<sup>c</sup>, Mario Zlatovic<sup>a</sup>, Dusan Sladic<sup>a</sup>, Thomas Vallet<sup>d</sup>, Marco Vignuzzi<sup>d,e</sup> and Radomir N. Saicic<sup>a,f</sup>

<sup>a</sup>Faculty of Chemistry, University of Belgrade, Belgrade, Serbia; <sup>b</sup>Innovation Centre of the Faculty of Chemistry, Belgrade, Serbia; <sup>c</sup>University of Belgrade-Institute of Chemistry, Technology and Metallurgy, Belgrade, Serbia; <sup>d</sup>Institut Pasteur, Center for the Viral Populations and Pathogenesis, Paris, France; <sup>e</sup>A\*STAR Infectious Diseases Labs (A\*STAR ID Labs), Agency for Science, Technology and Research (A\*STAR), Singapore, Singapore; <sup>f</sup>Serbian Academy of Sciences and Arts, Belgrade, Serbia

### ABSTRACT

We developed new iminosugar-based glycosidase inhibitors against SARS-CoV-2. Known drugs (miglustat, migalastat, miglitol, and swainsonine) were chosen as lead compounds to develop three classes of glycosidase inhibitors ( $\alpha$ -glucosidase,  $\alpha$ -galactosidase, and mannosidase). Molecular modelling of the lead compounds, synthesis of the compounds with the highest docking scores, enzyme inhibition tests, and *in vitro* antiviral assays afforded rationally designed inhibitors. Two highly active  $\alpha$ -glucosidase inhibitors were discovered, where one of them is the most potent iminosugar-based anti-SARS-CoV-2 agent to date ( $EC_{90} = 1.94 \mu\text{M}$  in A549-ACE2 cells against Omicron BA.1 strain). However, galactosidase inhibitors did not exhibit antiviral activity, whereas mannosidase inhibitors were both active and cytotoxic. As our iminosugar-based drug candidates act by a host-directed mechanism, they should be more resilient to drug resistance. Moreover, this strategy could be extended to identify potential drug candidates for other viral infections.

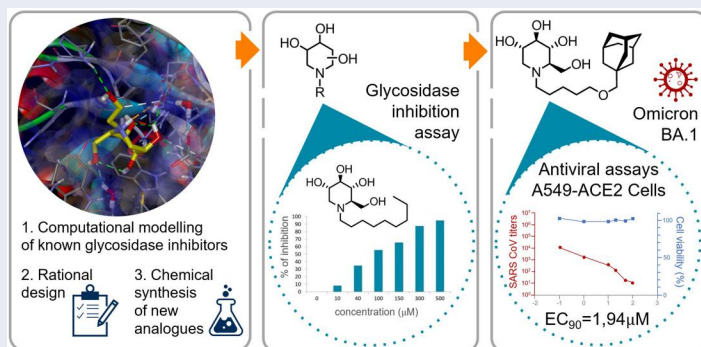
### ARTICLE HISTORY

Received 12 July 2023  
Revised 15 November 2023  
Accepted 24 November 2023

### KEYWORDS

COVID-19; antivirals; iminosugars; host-directed action; pandemic preparedness; glycosidase inhibitors

### GRAPHICAL ABSTRACT




## Introduction

Efficient protection of public health from infectious diseases involves the simultaneous application of non-pharmaceutical interventions, vaccination, and drugs. Even though the first two measures have been widely applied within the last 2 years, the COVID-19 pandemic and other viral diseases, such as Zika, dengue, Ebola, Rift Valley fever, yellow fever, measles, and West Nile, revealed the lack of suitable pharmacological responses except for HIV, HCV, and HBV<sup>1</sup>. Of the 80 antiviral drugs approved between 1987 and 2017, 68 were approved for the three aforementioned infections, whereas only 5 were approved for respiratory infections: 4 for influenza and 1 for RSV<sup>2</sup>. Moreover, drug repurposing<sup>3</sup> against

COVID-19 showed modest results<sup>4,5</sup>. The repurposed drugs remdesivir<sup>6</sup> and favipiravir (if administered in the early stage of the disease) shorten the recovery time and mitigate symptoms but do not affect the mortality rate<sup>7</sup>. The best clinically proven effect of a repurposed drug was for dexamethasone, which reduced mortality from severe COVID-19 by 30% (notably, dexamethasone is not an antiviral, but an anti-inflammatory drug)<sup>8</sup>. Most efforts to develop new drugs have focused on two therapeutic targets: viral proteases and polymerases. Two recently approved drugs against COVID-19, paxlovid<sup>9</sup> and molnupiravir<sup>10</sup>, inhibit Mpro and RdRp, respectively. However, the virus developed resistance to both drugs in a span of 2 months from the beginning of their distribution. In addition, the virus developed cross-resistance to the

**CONTACT** Radomir N. Saicic  [rsaicic@chem.bg.ac.rs](mailto:rsaicic@chem.bg.ac.rs)  Faculty of Chemistry, University of Belgrade, Belgrade, Serbia.

 Supplemental data for this article can be accessed online at <https://doi.org/10.1080/14756366.2023.2289007>.

© 2023 The Author(s). Published by Informa UK Limited, trading as Taylor & Francis Group.

This is an Open Access article distributed under the terms of the Creative Commons Attribution-NonCommercial License (<http://creativecommons.org/licenses/by-nc/4.0/>), which permits unrestricted non-commercial use, distribution, and reproduction in any medium, provided the original work is properly cited. The terms on which this article has been published allow the posting of the Accepted Manuscript in a repository by the author(s) or with their consent.

simultaneous action of both drugs, which is concerning because the simultaneous action of two drugs is commonly used to prevent cross-resistance<sup>11</sup>. Hence, new therapeutic agents with novel mechanisms of action are required for the efficient treatment of viral infections and protection of public health. Moreover, the therapeutic potential of these drugs should be preserved against mutated strains for a reasonable period.

The new series of drug candidates against COVID-19 should be efficient, available within a reasonable time, exhibit a general mechanism of action with a diverse antiviral activity, and prevent the onset of drug resistance. Hence, we selected the underexplored iminosugars, a class of potential host-directed antiviral agents<sup>12,13</sup>. Although iminosugars exhibited *in vitro* and/or *in vivo* activity against Ebola, Marburg<sup>14</sup>, dengue<sup>15</sup>, and SARS<sup>16</sup>, they have not been tested against COVID-19 to the best of our knowledge<sup>17,18</sup>.

Viral replication encompasses several phases, including the production of viral proteins in host cells. SARS-CoV-2 requires the host endoplasmic reticulum (ER) protein folding machinery for proper folding. Thus, selective inhibition of ER  $\alpha$ -glucosidases I and II, the key enzymes in glycoprotein processing, could be a promising mechanism of action for a COVID-19 drug<sup>19</sup>. Therefore, we selected known glucosidase I and II inhibitors as our first category of potential drug candidates. Miglustat (**1**, also known as *N*-butyldeoxyojirimycin, brand name Zavesca; Figure 1) is a clinically approved drug for the treatment of Niemann–Pick disease type C<sup>20</sup> and Gaucher disease type I<sup>21</sup>. Although its reported mechanism of action involves the inhibition of glucosylceramide synthase<sup>22</sup>, we presumed that miglustat may also act as an  $\alpha$ -glucosidase inhibitor owing to its structural similarity with glucose<sup>23</sup>. Moreover, deoxyojirimycin (**2**, DNJ, duvoglustat; Figure 1) is an EC 3.2.1.20 ( $\alpha$ -glucosidase) inhibitor as well as a pharmacological chaperone of acid  $\alpha$ -glucosidase<sup>24</sup> and has been tested against HIV, diabetes, and Pompe disease (a lysosomal storage disorder).

Moreover, mannosidases such as endo- $\alpha$ -1,2-mannosidase (MANEA) and Golgi  $\alpha$ -mannosidases I and II (MAN1A1 and GMII, respectively) can trim glycoproteins in the maturation phase. Therefore, we selected mannosidase inhibitors as our second category of potential drug candidates. As COVID-19 is primarily a respiratory disease and MANEA is not expressed or poorly expressed in the lung tissue, we focused our attention on Golgi mannosidases as potential therapeutic targets, with swainsonine (**3**, SWA; Figure 1), a known inhibitor of  $\alpha$ -mannosidase and mannosidase II, as a possible drug candidate<sup>25</sup>. Although swainsonine is not a clinically approved drug, its phase I and II clinical trials have been conducted and its toxicity data is available<sup>26</sup>.

Furthermore,  $\alpha$ -galactosidase A (GAL) has been identified as one of 66 potential drug targets from a SARS-CoV-2 protein interaction map<sup>27</sup>. Another study reported that galactosidase inhibitors are not active against dengue and Japanese encephalitis but show moderate activity against pestiviruses<sup>28</sup>. However, we believe that the strong interactions between the viral protein and

human GAL should be explored further. Deoxygalactonojirimycin (**4**, migalastat, DGJ, brand name Galafold; Figure 1), a clinically approved drug against Fabry disease (a rare metabolic disorder belonging to the group of lysosomal storage diseases), is a pharmacological chaperone for mutated GAL<sup>29</sup> but acts as GAL inhibitor at higher concentrations. Therefore, its activity against SARS-CoV-2 is worth exploring<sup>30</sup> and could be repurposed<sup>31</sup>. Hence, we selected GAL inhibitors as our third category of potential drug candidates for SARS-CoV-2.

Although drug repurposing accelerates drug development, repurposed drugs are rarely highly efficient for novel indications. Therefore, in this study, we developed an interactive and iterative process involving pharmacological analysis, molecular modelling, organic synthesis, and biological testing, where the candidates with repurposing potential were considered as lead compounds, whose antiviral activity and drug properties were optimised. First, we studied the known drugs miglustat, migalastat, and miglitol via interactive molecular modelling to discover new analogues. Then, we synthesised and tested some of these rationally designed  $\alpha$ -glucosidase, galactosidase, and mannosidase inhibitors for enzyme inhibition and anti-SARS-CoV-2 activities. Analysing enzyme inhibition activities is easier than that of anti-SARS-CoV-2 activity, and the correlation of both activities would aid in elucidating the mechanism of antiviral action and enhancing the antiviral activity.

## Results and discussion

### Modelling and designing the drug candidates

Our *in silico* study comprised four steps: 1) The crystal structure of the relevant glycosidase with a ligand was selected from the literature for docking studies; 2) The docking scores of several glycosidase inhibitor candidates were obtained and compared with experimentally observed inhibitory activity to check the feasibility of our model; 3) We chose an enzyme inhibitor clinically approved for another medical indication (e.g., miglustat, approved for the treatment of the Gaucher disease type I) and evaluated the docking of our glycosidase inhibitor candidates to the corresponding enzyme ( $\alpha$ -glucosidase II in this particular case); 4) Based on these results, we designed structural analogues with enhanced inhibitory activity.

### $\alpha$ -glucosidase inhibitors

A crystal structure of human ER glucosidase II bound to an inhibitor is not available in data banks, and the expression of this heterodimer has not been reported in the literature. However, the crystal structure of murine ER glucosidase II is available in the literature and would be suitable for our study<sup>32</sup>. Nevertheless, the glucosidase from *Chaetomium thermophilum* has been chosen for this study because: 1) it is a eukaryotic enzyme that has a similar active centre to that of the mammalian ones<sup>33</sup>; 2) its gene

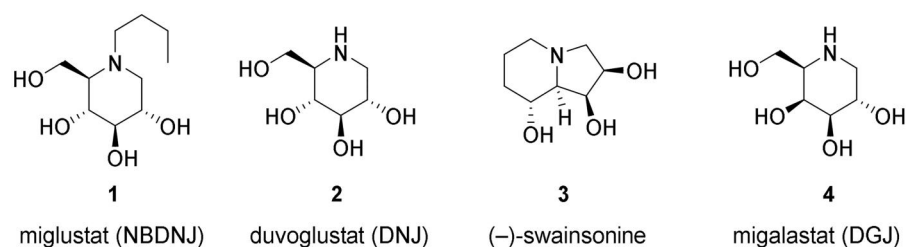
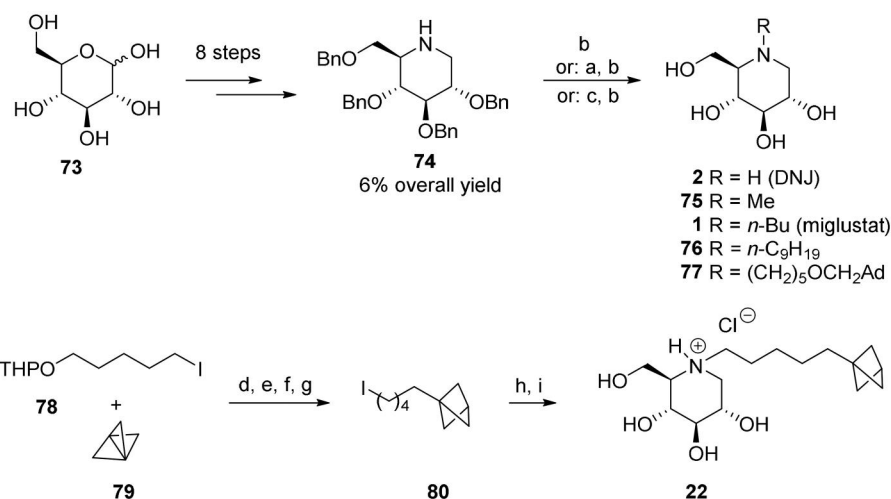
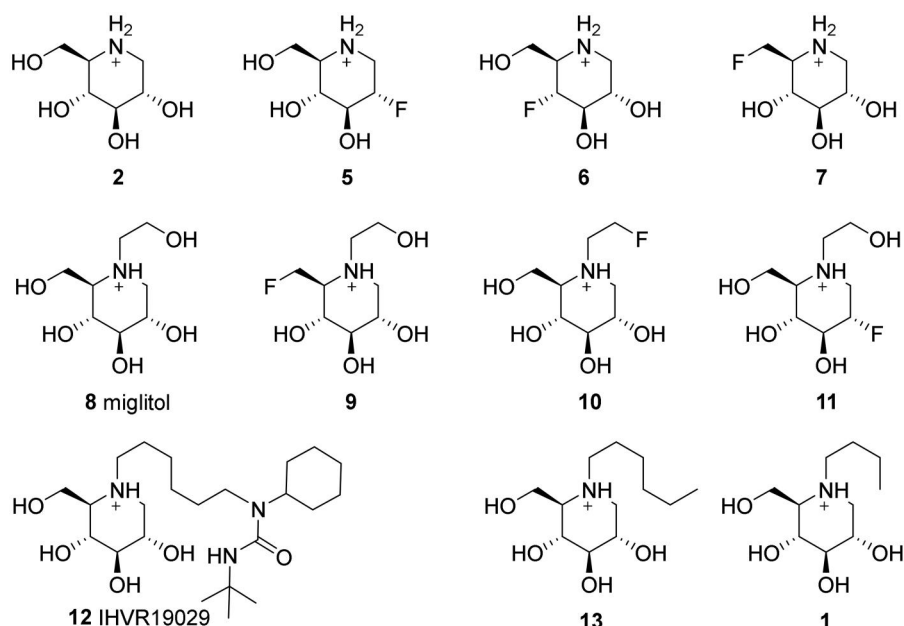


Figure 1. Selected glycosidase inhibitors that underwent clinical trials for various medical indications.



**Scheme 1.** Synthesis of deoxynojirimycin (DNJ)-derived  $\alpha$ -glucosidase inhibitors. Reagents and conditions: a) R<sup>1</sup>CHO, H<sub>2</sub> (1–4.2 atm), 10% Pd/C, 70–91%; b) H<sub>2</sub> (1–4.2 atm), 10% Pd/C, 70–100%; c) *n*-BuBr, K<sub>2</sub>CO<sub>3</sub>, DMF, 80 °C, 69%; d) MeLi, –40 °C, Et<sub>2</sub>O, 100%; e) TBTH, AIBN, PhH, 80 °C, 88%; f) *p*-TsOH, MeOH, 95%; g) PPh<sub>3</sub>, I<sub>2</sub>, imidazole, THF, 88%; h) **74**, K<sub>2</sub>CO<sub>3</sub>, DMF, 80 °C, 86%; i) H<sub>2</sub> (4 atm), Pd(OH)<sub>2</sub>/C, HCl, MeOH, 98%. Ad = adamantane-1-yl.



**Figure 2.** Structures and protonation states of the initial set of molecules at pH 7.00 ± 2.00, as predicted by the Epik module.

expression could be realised in *E. coli*;<sup>33b</sup> and 3) a good-quality crystal structure of this enzyme bound to a ligand,  $\alpha$ -D-glucopyranose-(1–3)- $\alpha$ -D-mannopyranose, is available. Because of our docking protocol, larger bioisosteric ligands were preferred as they would provide binding sites that can accommodate a variety of ligand structures.

The simulations were performed using the 5DL0<sup>34</sup> model as the target (selected from the RCSB protein database)<sup>35</sup>. The binding site was determined using a strong ER  $\alpha$ -glucosidase II inhibitor IHVR19029<sup>36</sup>. Then, a set of molecules (Scheme 1) were docked in their predicted protonation states at pH 7.00 ± 2.00 in water. All ligands were protonated at the given pH. We performed these experiments to 1) check the reliability of our docking procedure by comparing the calculated inhibitory activities with the experimental data from the literature and 2) identify the binding interactions that enhance and reduce inhibitory activity. Using this data, we designed ligands with superior binding properties.

Docking was performed on a small set of iminosugars (**1**, **2**, **5**–**13**) containing both polar and non-polar substituents at the N atom and isosterically replaced F atoms in the place of OH groups (Figure 2). The initial docking results indicated that the binding interactions of the piperidinium moiety were similar to that of IHVR-19029 (**12**) (Figure 3). The main interaction is the salt bridge between Asp633 and the protonated N atom of the iminosugar. Asp633 also acted as a H-acceptor in the H-bond with 3-OH, while Arg617 acted as a H-donor for the same OH group. Similarly, Asp443 formed two H-bonds as a H-acceptor with 4-OH and 2-hydroxymethyl group. The same hydroxymethyl group also formed H-bonds as a H-acceptor with water molecules at the binding site, thus engaging in indirect H-bonding with Trp517. Simulations showed that an *N*-substituent could increase the binding affinity depending on the length and nature of the substituent. The binding site is open towards the protein surface, where a non-polar “channel” was formed by Phe305, Phe563, Phe666, and

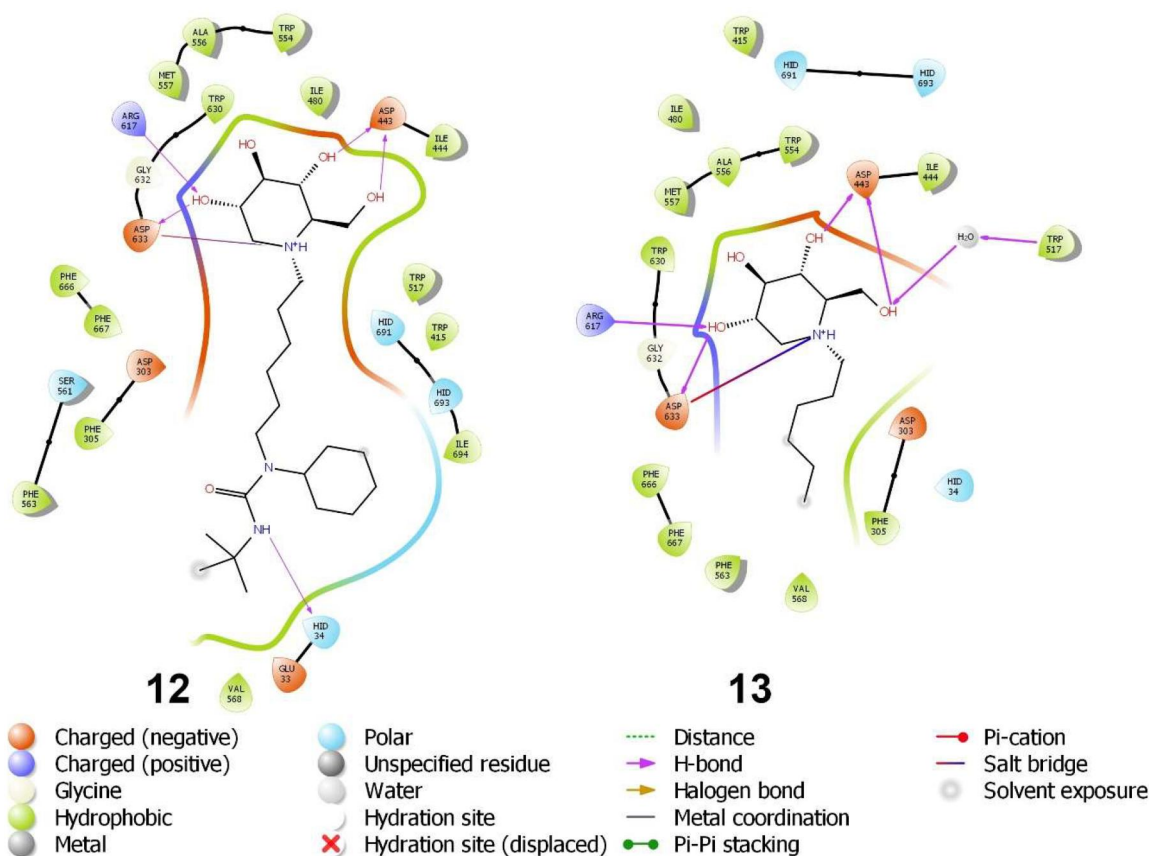


**Figure 3.** Binding interactions of small molecules with the binding site of endoplasmic reticulum (ER)  $\alpha$ -glucosidase II (5DL0).

**Table 1.** Docking scores of the investigated compounds after docking (left) and refining (right) as well as the previously reported data on  $\alpha$ -glucosidase inhibitors.

Docking			Refined scores			
Compound	Docking score	XP GScore	Compound	Docking score	XP GScore	Inhibitory activity
IHVR-19029	-10.379	-10.382	IHVR-19029	-11.154	-11.158	IC <sub>50</sub> = 27.8 $\mu$ M (pig liver) <sup>43</sup>
12			12			
1	-10.281	-10.285	8	-10.811	-10.855	IC <sub>50</sub> = 41.3 $\mu$ M (yeast) <sup>46</sup>
13			13			IC <sub>50</sub> = 9.88 mM (yeast) <sup>37</sup>
11	-10.263	-10.267	1	-10.617	-10.621	43.0 % at 1 mM (yeast) <sup>45</sup>
10	-10.042	-10.086	10	-10.468	-10.472	IC <sub>50</sub> = 13 $\mu$ M (rat liver) <sup>44</sup>
8			2			12.7 % at 1 mM (yeast) <sup>45</sup>
2	-9.713	-9.895	10	-10.091	-10.273	IC <sub>50</sub> = 16.73 mM (yeast) <sup>37</sup>
8	-9.637	-9.681	11	-10.042	-10.086	No literature data
2	-9.570	-9.582	2	-9.570	-9.582	K <sub>i</sub> = 25 $\mu$ M (yeast) <sup>40</sup>
6			9			K <sub>i</sub> = 21 $\mu$ M (yeast) <sup>41</sup>
5	-9.073	-9.076	6	-9.542	-9.722	K <sub>i</sub> = 7.0 $\mu$ M (pig liver) <sup>39</sup>
9	-8.760	-8.773	6	-9.073	-9.076	IC <sub>50</sub> = 16 $\mu$ M (rat liver) <sup>44</sup>
9	-8.652	-8.832	5	-9.073	-9.076	No activity (yeast) <sup>37</sup>
7	-8.610	-8.663	5	-8.760	-8.773	18 % at 5 mM (yeast) <sup>38</sup>
			7	-8.610	-8.664	K <sub>i</sub> = 2000 $\mu$ M (yeast) <sup>40</sup>
						K <sub>i</sub> = 19 $\mu$ M (yeast) <sup>40</sup>
						K <sub>i</sub> = 47 $\mu$ M (yeast) <sup>41</sup>
						K <sub>i</sub> > 5 mM (pig liver) <sup>39</sup>

Phe667 (non-polar aromatic) as well as Trp415 and Trp517 (aromatic with H-bonding ability), all of which have the potential for aromatic interactions. This structure accommodates the aliphatic chain of IHVR19209 (**12**), which can participate in H-bonding with His-34 or His693 owing to its flexibility. Docking simulations were repeated for molecules **1** (miglustat) and **13**. The results and docking scores confirmed the influence of the non-polar substituents.

These initial results were refined by redocking, which changed the ranking order, likely because of the minor steric clashes that were considered in this round. The inconsistencies between the relative positions of **8** and **11** in docking and refining could be a consequence of the energetically favourable intramolecular H-bond between the 2-hydroxyethyl and 4-OH groups. In this conformation, all the OH groups of **8** participated in ligand-protein or

intramolecular H-bonding, which lowers the total free energy of the protein–ligand complex. Molecules **13** and **1** also showed good docking results because of the additional hydrophobic interactions of the alkyl chain.

The comparison of the order of calculated binding affinities (according to our docking model) and the experimentally observed<sup>37–46</sup> order of inhibitory potencies (from the literature, Table 1) could not afford quantitative correlation between the docking scores and the inhibitory activities because the activity results were obtained in different studies, in which enzymes from various sources were used, as well as different substrates and reaction conditions, such as pH values. Besides that, the activities were expressed in various ways ( $K_i$ ,  $IC_{50}$  or percent of inhibition). This implies that only results from the same publication can be directly compared. We analysed the results in six publications<sup>37,39–41,44,45</sup>, but only qualitatively, since the maximum number of compounds studied in a particular publication was three. In five out of six above mentioned papers<sup>37,39,41,44,45</sup> higher docking scores corresponded to higher inhibitory activities. There was only one exception<sup>40</sup>, where compound **7** with the lowest docking score, showed higher activity than compounds **2** and **5** (relative activities of **2** and **5** are in accordance with their docking scores). It should be mentioned that the activities of **2** and **7** were determined in two other studies<sup>39,41</sup>, where they were in accordance with the order of our docking scores. Since, in most cases, a higher docking score corresponded to a higher inhibitory activity, we proceeded to use our model for guidance in designing human ER  $\alpha$ -glucosidase II inhibitors.

Subsequently, the hydrophobicity, potential aromatic and H-bonding interactions, and solvent-accessible surfaces (SASs) were examined. These visualisations (Figures are given in Supplementary Information) showed that in addition to the standard binding site at the piperidinium group, the entry channel is mainly hydrophobic and could participate in potential edge-to-face interactions. However, the exit of the binding site did not have any H-bond donors, and the SASs were large. Thus, a strongly binding ligand would have an aliphatic hydrophobic moiety in this region. This chain could also participate in aromatic interactions (C–H $\cdots\pi$ ) and even displace some water molecules from SAS if it is sufficiently long, increasing  $\Delta S$  and lowering the total energy of protein–ligand complex.

A bicyclopentyl (BCP) moiety at the end of an oligomethylene side chain would be suitable for such an interaction. The BCP group is metabolically stable and non-polar and can establish omnidirectional interactions similar to aromatic groups, as it is

bioisosteric to phenyl rings. Therefore, it has been used in lead compounds by some pharmaceutical companies<sup>47</sup>. Hence, we conducted docking simulations with three series of molecules containing the BCP moiety (Figure 4), where a H-acceptor O atom was introduced near the BCP moiety in two series.

Molecules with  $n=4, 5$ , and  $6$  showed the highest docking scores, comparable to that of the highest-ranked molecule tested, IHVR-19029 (**12**). The binding schemes and poses were similar to those of the previously tested molecules, with bicyclic moieties placed in a hydrophobic pocket consisting of Phe305, Trp517, Phe563, and Val568. The nature of the R substituent had no significant influence on the scores. The BCP participated in multiple  $\pi$ -alkyl interactions, justifying our selection (Figure 5; See Supplementary material for details). Based on these structures and their binding schemes, we presumed that molecules structurally similar to the adamantyl moiety could strongly bind to the target protein structure, and one such compound was selected for synthesis. In contrast, fluoro derivatives exhibited the lowest docking scores and hence were not considered for synthesis.

### GAL inhibitors

The modelling for  $\alpha$ -galactosidase A (GAL, EC 3.2.1.22) was performed using the human enzyme whose crystal structure has been previously reported (PDB ID: 6IBK)<sup>48</sup>. A set of compounds with known or presumed inhibitory activity were docked at the binding site of human GAL. This set of compounds included DGJ (**4**)<sup>29</sup>; azagalactofagomine (**40**, AGF; a strong  $\alpha$ -galactosidase inhibitor and potential drug candidate against Krabbe disease)<sup>49</sup>; meso-2,5-dihydroxymethyl-3,4-dihydropyrrolidine (**41**)<sup>50</sup>; 2,5-dideoxy-2,5-imino-D-altritol (**42**, DIA)<sup>50,51</sup>; and a series of BCP derivatives (**43–70**) with different side-chain lengths, heteroatom content, and substituents (Figure 6).

All simulations showed the same pattern. DGJ (**4**) exhibited the strongest binding, and its binding pose is characterised by strong salt bridges between the  $N^+$  and  $COO^-$  groups (Asp93, Asp170, Glu203, and Asp231), with additional  $\pi$ -cation interactions and H-bonds. The tested molecules with large substituents exhibited similar binding but lower binding scores. Even though **41** exhibited the key binding interactions, its binding score ( $-8.428$ ) was lower than that of DGJ ( $-9.312$ ). Furthermore, DIA (**42**) showed weaker binding and lower binding score ( $-6.156$ ) than that of **41**. Moreover, the  $pK_a$  prediction for AGF (**40**) showed that it is a neutral molecule ( $pK_a$  values of N atoms are  $4.98 \pm 0.98$  and  $4.41 \pm 0.98$  at physiological pH) with few interactions. Even though

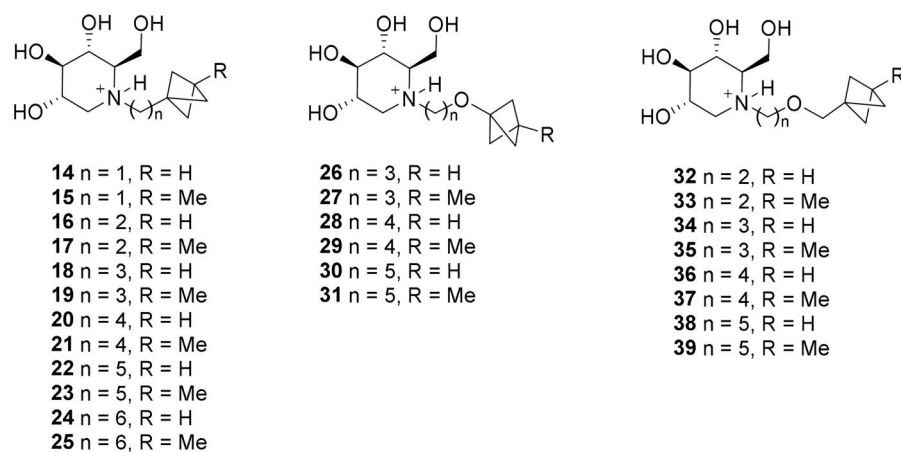
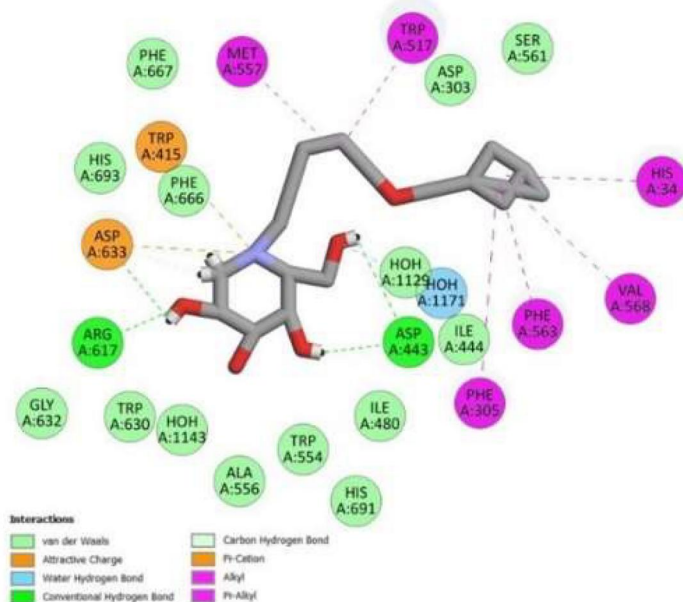


Figure 4. Structures and protonation states of the set of bicyclopentyl (BCP)-containing molecules at  $pH 7.00 \pm 2.00$ , as predicted by the Epik module.

A



B

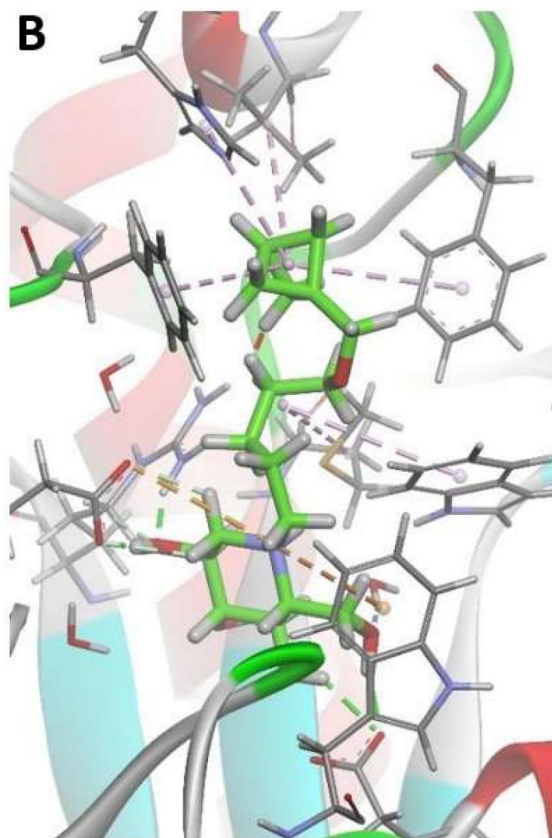


Figure 5. Interactions of ligands **26** (A) and **38** (B) at the binding site.

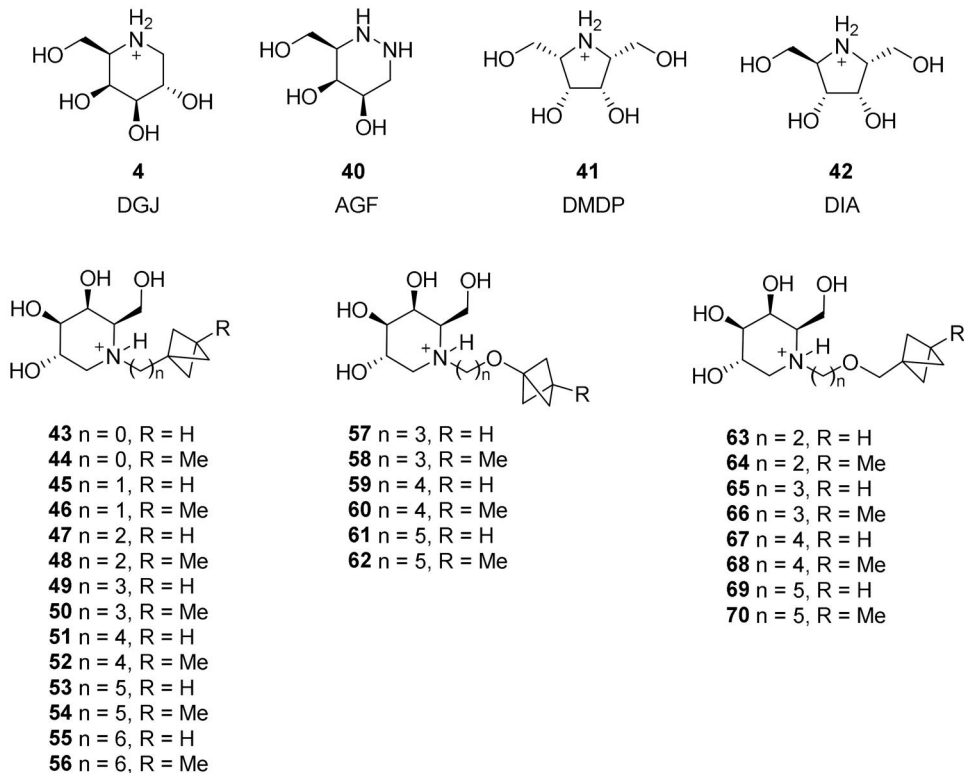


Figure 6. Presumed  $\alpha$ -galactosidase A (GAL) inhibitors.

we changed its protonation state by introducing alkyl substituents on the neighbouring N atom, its  $pK_a$  did not change significantly ( $\sim 0.2$ ).

In contrast, the general binding pattern was maintained for ligands with larger substituents (**43–70**), but the binding site in  $\alpha$ -galactosidase is shallow and lacks non-polar and/or aromatic

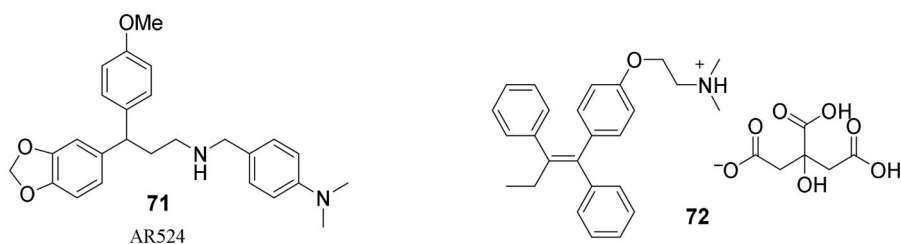


Figure 7. Non-iminosugar-type mannosidase inhibitors AR524 (**71**) and tamoxifen (**72**).

amino acids to stabilise alkyl-BCP substructure. Moreover, the disulphide bridge Cys142–Cys172 located opposite to the main binding site pushes out the longer *N*-substituents, disrupting the binding interactions at the main binding site. Molecules with longer chains showed lower binding scores (highest =  $-8.401$ ) than that of DGJ (**4**;  $-9.312$ ). Next, we experimentally evaluated these models using commercially available human  $\alpha$ -galactosidase, which is an advantage of our strategy.

### Mannosidase inhibitors

Human mannosidases relevant to SARS-CoV-2 replication, MAN1A1 and GMII, have not been characterised by X-ray crystallography thus far. Only the crystal structure of MANEA is available<sup>52</sup>; however, this enzyme is not expressed<sup>53</sup> or poorly expressed in the lung tissue<sup>54</sup>. Hence, we did not consider it for modelling. Instead, we chose swainsonine (**3**), a known inhibitor of GMII. Furthermore, a literature search identified a new class of compounds with anticancer properties (notably AR524; **71**, Figure 7) that act by inhibiting spheroid formation and interfering with glycoprotein processing via mannosidase inhibition<sup>55</sup>. As SARS-CoV-2 enters a cell by binding the RBD to the ACE2 receptor (both heavily glycosylated), AR524 might interfere with the replication cycle and exhibit antiviral activity. Moreover, tamoxifen (**72**; brand name: Nolvadex; Figure 7)<sup>56</sup>, an adjuvant therapeutic agent for hormone-dependent tumours, may also act via a mannosidase-inhibiting mechanism (although this is unlikely to be the main mechanism of action)<sup>57</sup>. Therefore, we included tamoxifen (**72**) and AR524 (**71**) in this category even though they are structurally unrelated to iminosugars.

### Synthesis of the drug candidates

#### $\alpha$ -Glucosidase inhibitors

DNJ was used as the heterocyclic core in the analogues with modified side chains. A protected DNJ derivative **74** (the key intermediate) was prepared from glucose **73** using the chiron approach and a modified previously reported method<sup>58</sup>. Next, various *N*-substituted analogues (**1**, **2**, **75**, **76**, **77**, **22**) were prepared by alkylation or reductive amination (Scheme 1). The BCP analogue **22** comprises a linker of the appropriate length (five methylene units, as suggested by calculations) between the BCP fragment and the heterocyclic core. Notably, its synthesis method involving the positioning of BCP fragment suitably could be extended to synthesise other compounds containing BCP fragment, which is a significant bioisostere in medicinal chemistry<sup>47</sup>

#### $\alpha$ -galactosidase a inhibitors

DGJ (**4**), the most potent among the known  $\alpha$ -galactosidase inhibitors, was synthesised via a tandem organocatalyzed aldol addition/reductive amination (Scheme 2, Equation 1)<sup>59</sup>. The reduced

analogue **93** (4-epi-fagomine) was prepared in a similar manner (Scheme 2, Equation 2)<sup>60</sup>. These compounds were then converted into a series of *N*-alkylated analogues via reductive amination, as described in the previous section for the DNJ analogues. The alkylation of **85** with iodide **80** afforded a mixture of **95** and **96** owing to the migration of the TBS group (Scheme 2, Equation 3). However, this result was inconsequential as only a single product **53** was formed after deprotection.

The tandem organocatalyzed aldolisation/reductive amination afforded efficient access to the pyrrolidine derivatives **41** and **42** (DIA)<sup>59</sup>. The aldolisation step proceeds under reagent control, which allows the production of both compounds from the squalemic starting aldehyde **97** (Scheme 3).

Azagalactofagomine (AGF; **40**) was obtained by a similar procedure, except for the substitution of reductive hydrazination in place of reductive amination<sup>61</sup>; to the best of our knowledge, this is only the second example of such an intramolecular reaction in the literature (Scheme 4)<sup>62</sup>. Moreover, the reductive hydrazination of derivative **102** with formaldehyde followed by deprotection afforded the methylated analogue **104**.

### Mannosidase inhibitors

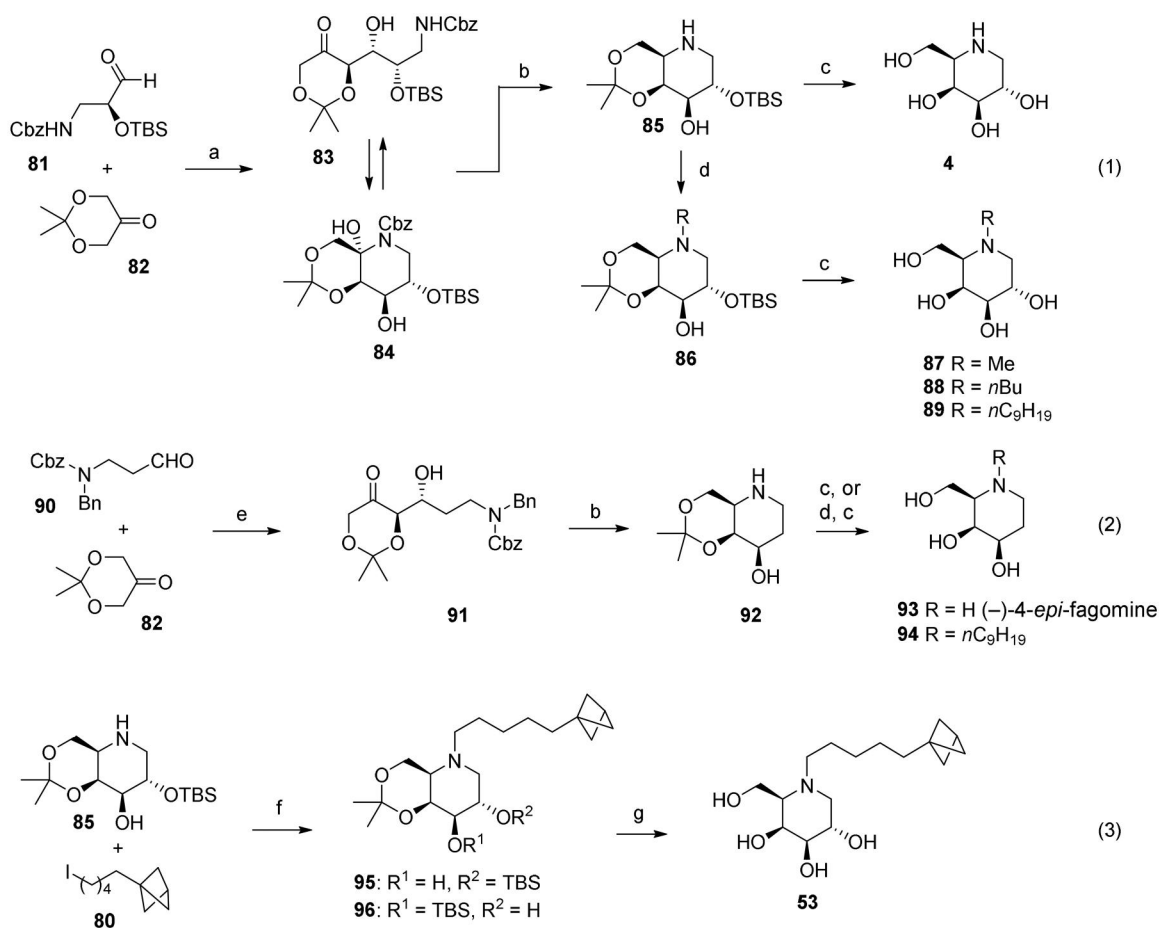
(–)-Swainsonine (**3**) was obtained via a previously developed method for the synthesis of the (+)-enantiomer (Scheme 5)<sup>63</sup>. Compound AR 524 (**71**) was prepared using a previously reported method<sup>55</sup>, whereas tamoxifen (**72**) was obtained from commercial sources.

### Enzyme assays

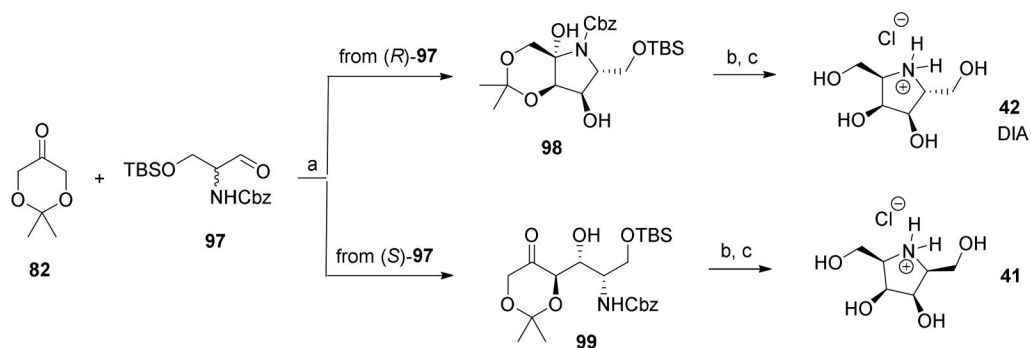
Assuming that the inhibition of glycoprotein is the principal mode of the antiviral activity of iminosugar<sup>64</sup>, we conducted enzyme assays as a proxy to anti-SARS-CoV-2 activity.

In the case of the  $\alpha$ -glucosidase inhibitors, we initially attempted to express the gene for *Chaetomium thermophilum* ER glucosidase II in *E. coli*<sup>65</sup> and evaluate the inhibitory potency of DNJ and its derivatives, which have a similar structure to that of glucose<sup>66</sup>. However, the purified cloned protein did not exhibit enzymatic activity,<sup>33b</sup> whereas the cell lysate had insufficient enzymatic activity to obtain reliable results. To overcome this issue, we expressed recombinant *Saccharomyces cerevisiae* (*S. cerevisiae*)  $\alpha$ -glucosidase in *E. coli*<sup>65</sup>. Although a mammalian enzyme would be the best option, other eukaryotic enzymes can be considered as appropriate targets, as the sequences of both the  $\alpha$ - and  $\beta$ -subunits of ER  $\alpha$ -glucosidase II are highly conserved in eukaryotes<sup>32</sup>. In addition, the  $\alpha$ -subunit of yeast glucosidase II is similar to the human one, and the only role of the  $\beta$ -subunit (which does not exist in yeast) is to position the enzyme within the ER, which is unnecessary for the enzyme inhibition test and justifies its use as a proxy for human  $\alpha$ -glucosidase II<sup>66</sup>. A synthetic gene encoding  $\alpha$ -glucosidase from *S. cerevisiae* was inserted into a





**Scheme 2.** Synthesis of deoxygalactonojirimycin (DGJ) and its analogues. Reagents and conditions: a) (*R*)-Pro (cat.), DMF, rt, 61%; b) H<sub>2</sub> (4.5 atm), 10% Pd/C, EtOH, 75%; c) HCl, MeOH, 70–90%; d) RCHO, H<sub>2</sub> (1–4 atm), 10% Pd/C, EtOH, 54–94%; e) (*R*)-Pro (cat.), DMF, 4 °C, 24 h, 60%; f) K<sub>2</sub>CO<sub>3</sub>, DMF, 80 °C, **95** : **96** = 2 : 1, 94% total yield; g) HCl, MeOH, 50%.

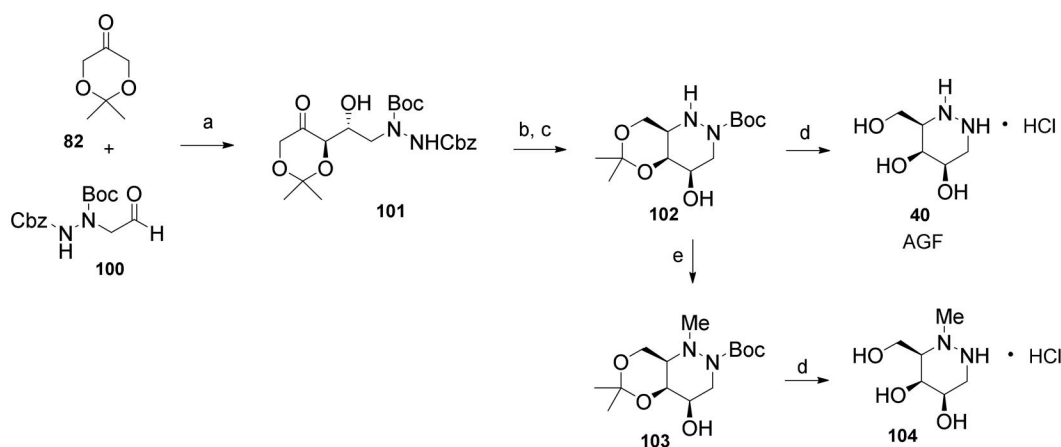


**Scheme 3.** Synthesis of pyrrolidine derivatives **41** and **42**. Reagents and conditions: a) (*R*)-Pro (cat.), DMF, 4 °C, 48 h, **98**: 37%, **99**: 33%; b) H<sub>2</sub> (4.5 atm), 10% Pd/C, EtOH; c) 3 M HCl, MeOH, **42**: 43% over 2 steps, **41**: 55% over 2 steps.

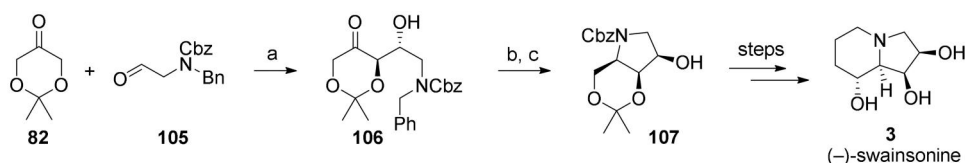
pET-22b(+) vector to produce recombinant protein in the cytosol of *E. coli*<sup>65</sup>. The inhibition of yeast  $\alpha$ -glucosidase by the iminosugar library compounds (0–500  $\mu$ M) was determined using *p*-nitrophenyl  $\alpha$ -D-glucopyranoside as the substrate<sup>67</sup>. A linear dependence was observed between log *c* and the percentage of inhibition; a representative example is shown in Figure 8, and the IC<sub>50</sub> values of the tested compounds are shown in Table 2.

All tested compounds showed inhibitory activity against the enzyme. The highest activity was exhibited by DNJ, but the derivatives with longer N chains had similar IC<sub>50</sub> values. Notably, compounds with short alkyl chains with or without polar substituents exhibited lower activity. These results can be rationalised by

considering the mechanism of action of  $\alpha$ -glucosidases<sup>68</sup>. Iminosugars can be regarded as analogues of oxonium ion-like transition states, with protonated N instead of positive O. Hence, a short alkyl chain, with or without a hydroxyl group, may not be able to provide an additional binding interaction while simultaneously shielding the positive centre, which lowers the degree of inhibition. In contrast, longer hydrophobic chains, while still shielding the protonated nitrogen, bind to an auxiliary binding site (the hydrophobic channel) by interacting with non-polar and aromatic amino acid side chains, thereby increasing the binding constant and, consequently, the inhibition potency. Moreover, these results are confirmed by our computational modelling



**Scheme 4.** Synthesis of azagalactofagomine (AGF) and its methylated derivative. Reagents and conditions: a) (*S*)-Pro, DMSO, H<sub>2</sub>O, 53%; b) H<sub>2</sub> (1 atm), 10% Pd/C, MeOH, rt, 1 h; c) NaBH<sub>3</sub>CN, AcOH, MeOH, rt, 30 min, 65% over 2 steps; d) 3 M HCl<sub>(aq)</sub>, MeOH, rt, 24 h, **40**: 96%; **104**: 100%; e) HCHO<sub>(aq)</sub>, H<sub>2</sub> (1 atm), Pd(OH)<sub>2</sub>/C, EtOAc, AcOH, rt, 6 h, 84%.



**Scheme 5.** Synthesis of (-)-swainsonine (**3**). Reagents and conditions: a) (*R*)-Pro (cat.), DMF, 66%; b) H<sub>2</sub>, Pd/C (10%), MeOH; c) CbzCl, Et<sub>3</sub>N, THF (71% over 2 steps).

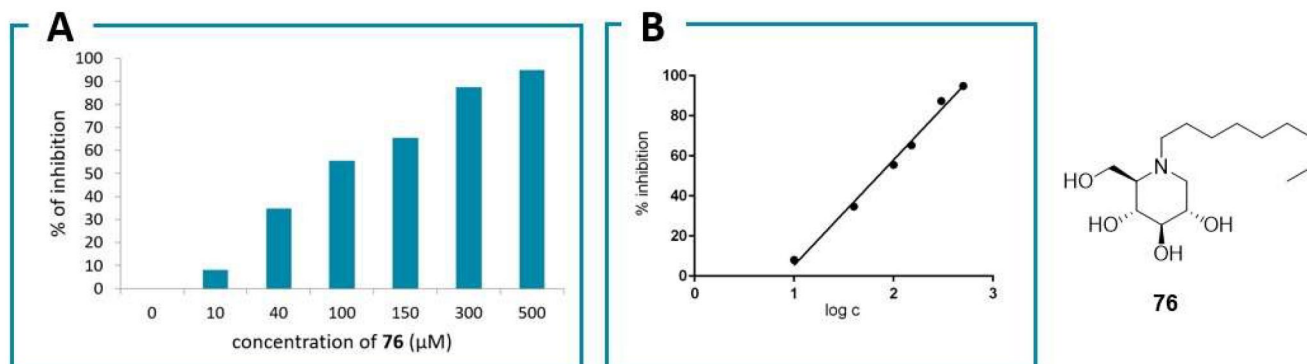


**Figure 8.** Dependence of the percentage of inhibition on concentration (A) and log *c* (B) of **76**.

results, where longer hydrophobic chains led to higher docking scores than those of shorter chains. Notably, the adamantyl derivative **77** that exhibited the highest inhibitory potency among the *N*-substituted derivatives also had the highest docking score. However, the experimental and computational data exhibited some differences, which could be attributed to the use of different enzymes for docking and the inhibition assay. Although eukaryotic  $\alpha$ -glucosidase sequences are highly conserved, previous studies have shown relatively large discrepancies between the iminosugar inhibition data. For example, miglitol, which showed low activity in this study, strongly inhibited  $\alpha$ -glucosidase activity in rice ( $IC_{50} = 0.05 \mu\text{M}$ ) and weakly inhibited  $\alpha$ -glucosidase in yeast ( $IC_{50} > 1000 \mu\text{M}$ )<sup>69</sup>. Moreover, miglustat (**1**), which showed weak activity against the yeast enzyme in this study, showed strong activity against ER glucosidase II ( $IC_{50} = 13 \mu\text{M}$ ), intestinal and lysosomal  $\alpha$ -glucosidases, and an intestinal  $\beta$ -glucosidase<sup>44</sup>. This lack of selectivity is not desirable owing to potential side effects. Furthermore, DNJ previously showed strong activity against ER glucosidase II ( $IC_{50} = 16 \mu\text{M}$ ) without selectivity, which is comparable to the activity observed in this study. Compound **76** previously exhibited higher activity than miglustat (**1**) or DNJ (**2**)

against mouse ER  $\alpha$ -glucosidase II without selectivity<sup>23</sup>. Thus far, only a tocopherol-DNJ conjugate selectively inhibited ER  $\alpha$ -glucosidase II<sup>44</sup>; however, it accumulates in the liver due to extreme lipophilicity and thus is unsuitable for the treatment of respiratory diseases despite its potential as an anti-flaviviral agent. Hence, all the synthesised DNJ analogues emerged as promising antiviral drug candidates.

Next, the inhibitory activity of the potential GAL inhibitors was measured using a commercial recombinant human enzyme with *p*-nitrophenyl  $\alpha$ -D-galactopyranoside as the substrate via a previously reported method<sup>67</sup>. The results are presented in Table 3, and concentration-dependent inhibition is shown in Figure 9 (Full data for other inhibitors are provided in the Supplementary material).

All the compounds showed some level of activity at the highest concentration (100  $\mu\text{M}$ ). Some compounds were highly active and exhibited structure-activity relationships. DGJ (**4**), the parent compound of the piperidine series, exhibited the highest activity against GAL. Moreover, as expected, the GAL inhibitors with short alkyl chains (methyl and butyl) exhibited higher activity than those with long alkyl chains owing to the shallow binding site.

**Table 2.** IC<sub>50</sub> values of the yeast  $\alpha$ -glucosidase inhibitors.

Compound	IC <sub>50</sub> / $\mu$ M	
1	$\geq 500$	
2	54	
8	$\geq 500$	
22	218	
75	572	
76	70	
77	67	

**Table 3.** IC<sub>50</sub> values of the human  $\alpha$ -galactosidase inhibitors.

Compound	IC <sub>50</sub> / $\mu$ M	
4	0.17	
40	$\geq 100$	
41	1.0	
42	5.0	
53	59.3	
87	5.1	
88	24.4	
89	$\geq 100$	
93	$\geq 100$	
94	$\geq 100$	
104	$\geq 100$	

However, the BCP analogues showed some auxiliary binding with aromatic residues as BCP is bioisosteric to phenyl group. 2-Deoxy-DGJ (**93**) and its nonyl derivative **94** as well as AGF (**40**) and its methyl derivative **104** showed low activity, irrespective of the presence of an *N*-substituent. The latter result was consistent with the computational results, which predicted a low fraction of protonated molecules. Furthermore, both pyrrolidine stereoisomers were highly active, where the *meso*-galacto derivative showed a slightly higher activity (**41**; IC<sub>50</sub> = 1.0  $\mu$ M) than the *D*-altro derivative (**42**, DIA; IC<sub>50</sub> = 5.0  $\mu$ M). A similar trend was observed for **41**

and **42** (IC<sub>50</sub> = 0.19 and 5.2  $\mu$ M, respectively) in a previous study on the inhibition of  $\alpha$ -galactosidase in coffee beans<sup>50</sup>.

Finally, four compounds, the pyrrolidine derivatives **41** and **42** (DIA), the most active piperidine derivative **4** (miglustat, DGJ), and the parent 1,2-diazinane **40** (AGF) were chosen for *in vitro* antiviral assays.

### *In vitro* assays

*In vitro* assays were performed using standardised protocols established at the Institut Pasteur to evaluate antiviral compounds in

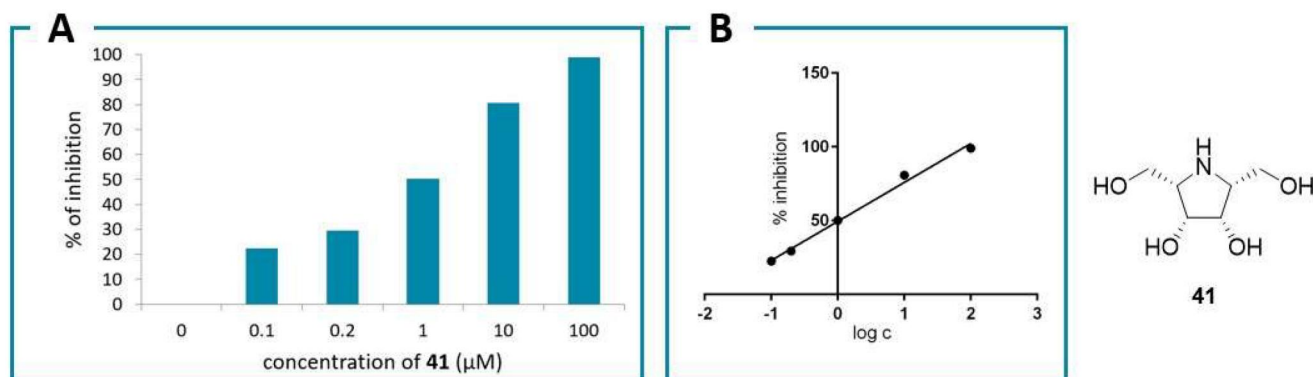


Figure 9. Dependence of the percentage of inhibition on concentration (A) and log c (B) of 41.

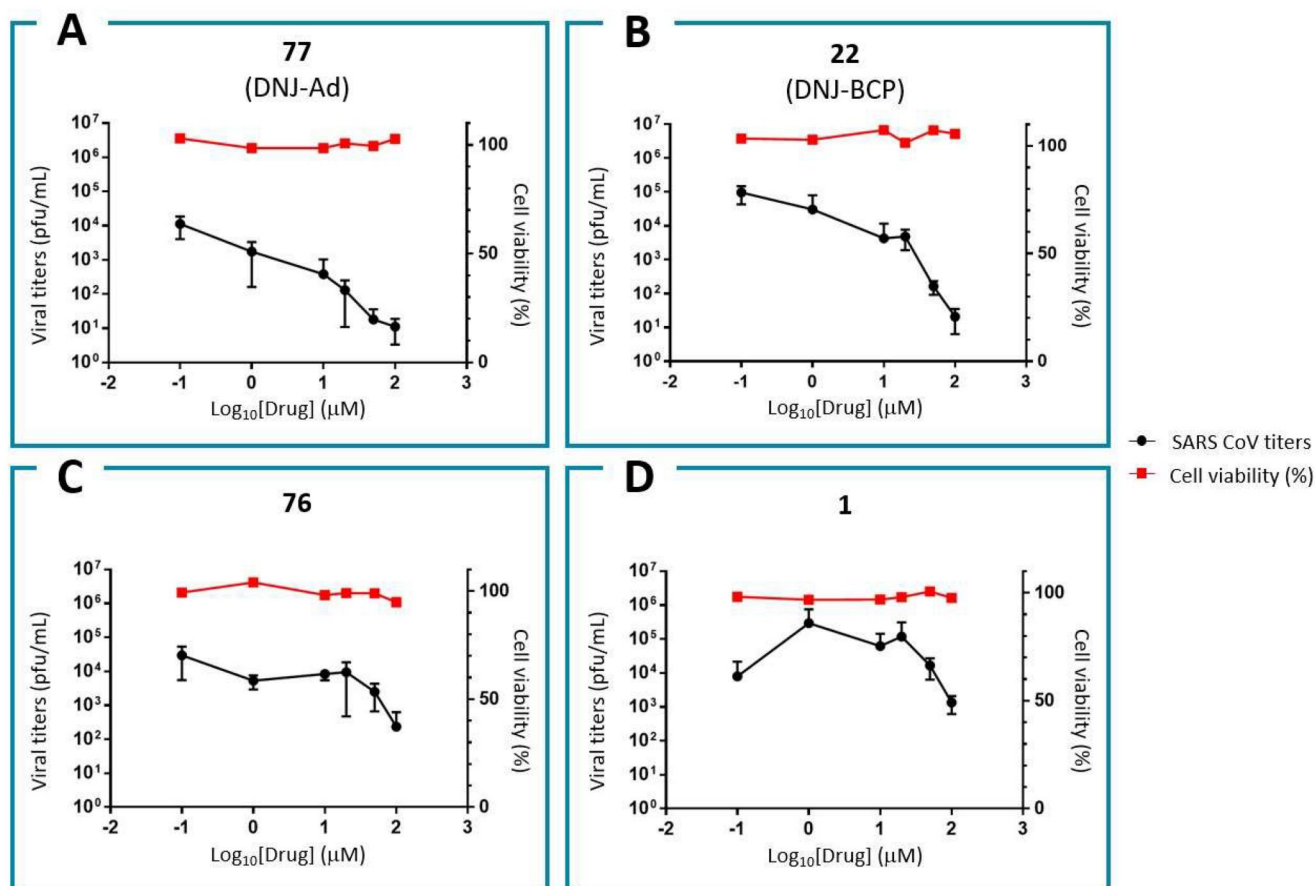


Figure 10. Anti-SARS-CoV-2 activities and cytotoxicities for  $\alpha$ -glucosidase II inhibitors: 77 (A), 22 (B), 76 (C) and 1 (D).

cell cultures during the pandemic, which involved the use of a robust and reproducible low-to-medium throughput method.

Even though glucosidase inhibitors are regarded as potential anti-SARS-CoV-2 agents<sup>17,70</sup>, their anti-SARS-CoV-2 activities had not been reported before beginning this study. However, since then, six studies have reported the anti-SARS-CoV-2 activities of glucosidase inhibitors. Rosenzweig et al. observed that miglustat induces structural changes in SARS-CoV-2 and the host proteins but does not exhibit a significant therapeutic effect<sup>71</sup>. However, they focused on the early stages of the viral infection (fusion) but not on replication. Hence, their report could be considered insufficient evidence<sup>72</sup>. Marcello et al. reported that miglustat has moderate anti-SARS-CoV-2 activity ( $EC_{50} = 41 \pm 22 \mu\text{M}$ ) and celgosivir

(a prodrug of castanospermine) showed high activity ( $EC_{50} = 1 \pm 0.2 \mu\text{M}$ ) in Vero E6 cells<sup>73</sup>. However, a later study reported that chloroquine protected only Vero E6 cells from SARS-CoV-2 infection but not Calu3 or model cells for respiratory infections<sup>74</sup>. Hence, the VeroE6 cell line may not be suitable to analyse *in vitro* anti-SARS-CoV-2 activity. Bradfute et al. reported that celgosivir, castanospermine, and UV-4 (10–100  $\mu\text{M}$ ) helped SARS-CoV-2-infected Vero E6 cells; however, the antiviral effect was lost after 48 h<sup>75</sup>. Recently, Brown et al. showed that UV-4 demonstrated strong anti-SARS-CoV-2 activity in A549-ACE2 cells ( $EC_{50} = 4 \mu\text{M}$ )<sup>76</sup>. Block et al. reported that IHVR 19029 (**12**) exhibited high activity against SARS-CoV-2 in A549-ACE2 cells ( $EC_{90} = 4 \mu\text{M}$ )<sup>77</sup>, whereas Mariuzza et al. reported several ER  $\alpha$ -glucosidase I

inhibitors for SARS-CoV-2 with  $EC_{50}$  values at the submicromolar level, where the most potent compound EB-0128 has an  $EC_{50}$  of  $0.42 \mu\text{M}$ <sup>78</sup>.

In this study, we tested seven DNJ analogues for SARS-CoV-2 activity, and the results of the four highest antiviral activities are shown in Figure 10. The other results are shown in Figure S42. The activity of miglustat ( $EC_{90} = 100 \mu\text{M}$ ) was consistent with previous reports. Notably, **77** exhibited the highest anti-SARS-CoV-2 activity ( $EC_{90} = 1.94 \mu\text{M}$ ;  $EC_{50} = 0.23 \mu\text{M}$ ), which is consistent with its high docking score ( $-11.471$ ), and thus is the most potent anti-SARS-CoV-2 agent from the iminosugar family (Figure 10A). Moreover, **77** was previously reported as a selective inhibitor of non-lysosomal glucosylceramidases (including  $\beta$ -glucosidase 2) and was regarded as inactive towards ER glucosidases involved in *N*-glycan trimming<sup>79</sup>. This assumption was based on its lack of activity against the influenza haemagglutinin folding process in ER, where inhibition occurred only at a  $200 \mu\text{M}$  concentration of **77**. We believe that this does not reflect a lack of activity but rather virus-specific sensitivity towards the inhibition of the glycoprotein maturation step, as influenza is apparently more resilient than SARS-CoV-2.

In addition, BCP derivative **22** exhibited strong antiviral activity ( $EC_{90} = 3.83 \mu\text{M}$ ), although weaker than that of **77** (Figure 10B). Its activity could be further improved. Compound **76** also exhibited moderate activity ( $EC_{90} = 45 \mu\text{M}$ ). Notably, no cytotoxicity was observed towards the used cells for any of the tested agents at  $EC_{90}$  concentrations. These results were obtained with A549-ACE2 lung carcinoma epithelial cells that express the ACE2 virus receptor, relevant for the COVID infection, and with the Omicron BA.1 viral strain. As Omicron is currently the dominant form of SARS-CoV-2, both the cell type and the viral strain are pertinent for the evaluation of therapeutic potential.

Researchers have attempted to develop selective inhibitors of ER  $\alpha$ -glucosidase I or II to avoid side effects<sup>15,44,78</sup>. In particular, although we believe that inhibition of lysosomal and/or gastrointestinal glucosidases should be avoided, selectivity between ER  $\alpha$ -glucosidase I and II is not required because both enzymes participate in glycoprotein maturation and a bi-pronged inhibition would increase the antiviral potency of the drug. Moreover, even though Mariuzza et al. developed selective inhibitors of ER  $\alpha$ -glucosidase I, they observed that the strongest antivirals exhibit cross-inhibition of both  $\alpha$ -glucosidase I and II<sup>78</sup>.

These results confirm our previous structure-activity relationships (SAR) analysis, which revealed that an active inhibitor should possess a DNJ head and a flexible aliphatic side chain with large substituents capable for aromatic/non-polar interactions at the chain-terminal. The decreasing potency in the order of **77** > **22** > **76** > **1** affirms the importance of their non-polar/aromatic interactions with the aromatic amino acids in the hydrophobic pocket of  $\alpha$ -glucosidase II containing Phe305, Phe563, His34, and Val568. The positions of the ligands **1**, **76**, **22**, and **77** and their interactions with the aforementioned amino acids in the binding pocket are shown in Figure 11. Compound **76** was more active than miglustat **1** because of its longer alkyl chain and hence exhibits six hydrophobic interactions in contrast to the two hydrophobic interactions observed for **1** (Table S1). The BCP fragment in **22** acts as an isotropic phenyl ring isostere, whose H atoms engage in CH- $\pi$  H-bonding with the aforementioned amino acids more efficiently than ordinary  $sp^3$  H atoms from a straight alkyl chain (butyl chain in **1** or the nonyl chain in **76**) owing to the strain-induced hybridisation change. The adamantyl subunit in the most active compound **77** with its octupole and high dipole polarizability is an even better H-donor in the CH- $\pi$  bonds with Phe305, Phe563, and His34. In addition, owing to its spherical symmetry, the adamantyl moiety of **77** participates in more hydrophobic interactions than the aliphatic chains. Furthermore, **77** exhibits intramolecular hydrophobic interactions, which makes the side-chain conformation more rigid than those in **1**, **22**, and **76**. Due to this side chain shortening, the adamantyl subunit does not interact with Val568 like **22** and **76** do; however, this lack of interaction is compensated by stronger interactions with Phe305, Phe563 and His34, as explained previously. Additionally, the role of His34 depends on the ligand structure, where **22**, **76**, and **77** participate in hydrophobic interactions and **12** (IHVR 19029) acts as a H-bond acceptor (Figure 3).

In the case of the GAL inhibitors, none of the four tested samples were active against SARS-CoV-2, which is contrary to previous reports on their potential for viral protein-host protein interactions<sup>27,31</sup>.

In the case of the mannosidase inhibitors, (-)-swainsonine **3** and **71** showed significant antiviral activities ( $EC_{90} = 50$  and  $20 \mu\text{M}$ , respectively; Figure 12 A and B). However, they also showed cytotoxicity at  $EC_{90}$  concentrations, which precludes their therapeutic use. Moreover, tamoxifen **72** showed high antiviral

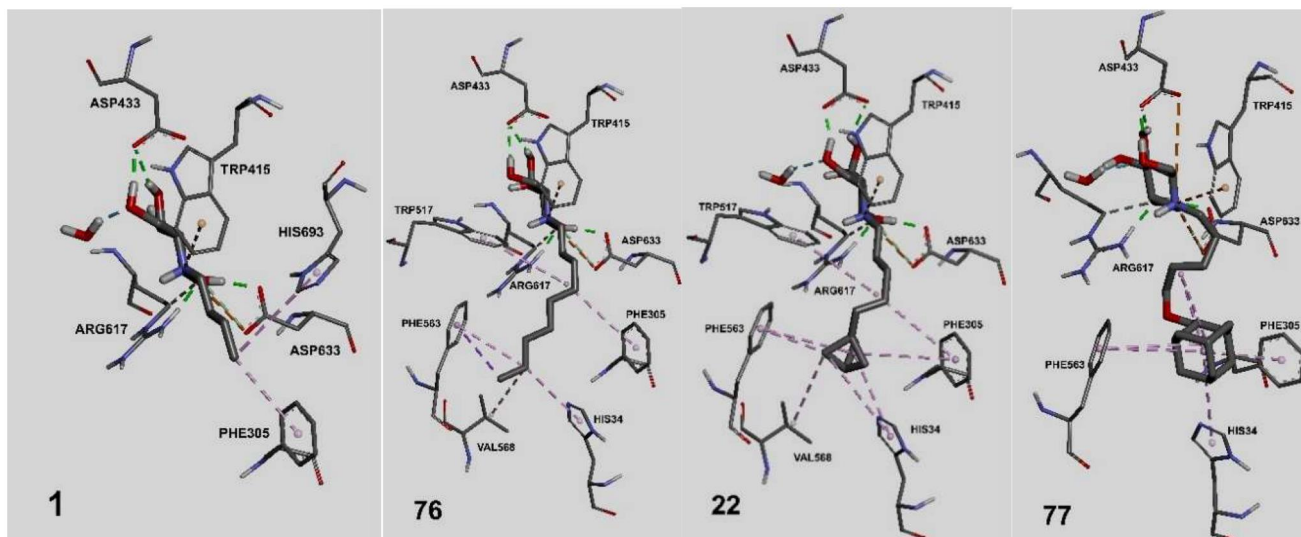
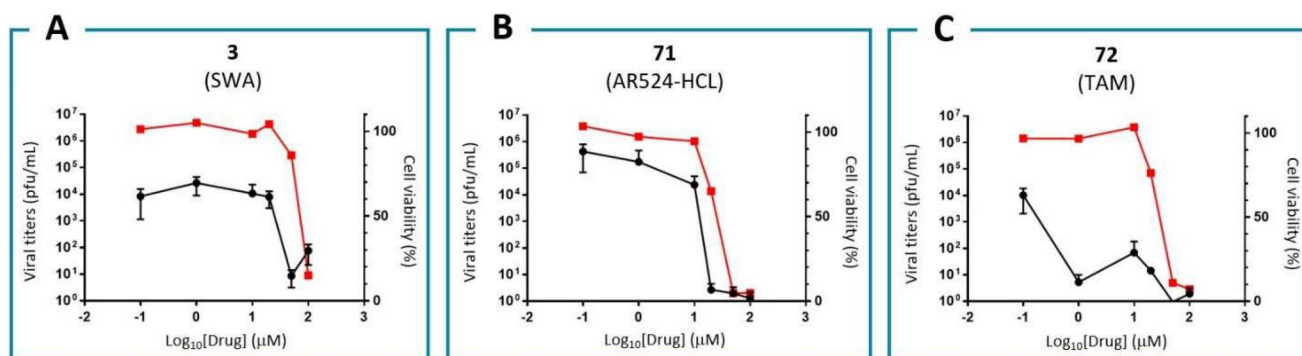


Figure 11. Interactions of ligands **1**, **76**, **22**, and **77** in the binding site of  $\alpha$ -glucosidase II.



**Figure 12.** Antiviral activities and cell viabilities of mannosidase inhibitors: (–)–swainsonine (3, A), 71 (B), and tamoxifen (72, C).

activity ( $EC_{90} < 1 \mu\text{M}$ ) and cytotoxicity only at 100-fold higher concentrations (Figure 12C). Hence, it is an excellent candidate to be repurposed for SARS-CoV-2. Our results are supported by a report by Yang et al., where they confirmed the anti-SARS-CoV-2 activity of tamoxifen and its structurally related clomiphene<sup>80</sup>. However, the mechanism of action of tamoxifen should be elucidated in a future study, as it is only assumed that it affects glycoprotein processing.

## Conclusion

In this study, we designed, synthesised, and conducted *in vitro* studies of three classes of iminosugar-based glycosidase inhibitors as potential anti-SARS-CoV-2 agents. Two  $\alpha$ -glucosidase inhibitors inhibited the replication of SARS-CoV-2 *in vitro*, where one of them (77) is the most potent iminosugar-based anti-SARS-CoV-2 agents reported thus far ( $EC_{90} = 1.94 \mu\text{M}$  in A549-ACE2 cells against Omicron BA.1 strain). The presence of a BCP fragment in the side chain (22) increased the potency of the drug ( $EC_{90} = 3.83 \mu\text{M}$ ). SAR studies showed that the hydrophobic interactions of the antiviral agents with the amino acids Phe305, Phe563, His34, and Val568 should be maximised to enhance the inhibitor activity and to develop a 2<sup>nd</sup> generation of analogues<sup>81</sup>. However, GAL inhibitors showed no antiviral effects, whereas mannosidase inhibitors were both antiviral and cytotoxic. Notably, tamoxifen emerged as a strong candidate for repurposing, but further elucidation of its mechanism of action is required. The principle of host-directed action that we applied to identify potential anti-SARS-CoV-2 agents could be applied to other viruses. Research in this direction is currently ongoing in our laboratory.

## Experimental

### Molecular docking simulations

All protein structures ( $\alpha$ -glucosidase II, PDB ID: 5DL0<sup>34</sup>;  $\alpha$ -galactosidase A, PDB ID: 6IBK)<sup>48</sup> were prepared using the Protein Preparation Wizard from the Schrödinger Suite 2021–1<sup>82</sup>. All small molecules were designed in Maestro module from Schrödinger<sup>83</sup>. To determine their correct protonation states at given pH, all molecules were submitted to Epik module from Schrödinger Suite<sup>84</sup>. In this case, pH was set to  $7.00 \pm 2.00$  in water. All molecules were docked in state predicted by Epik. Molecular docking simulations on protein models were performed in Glide module from Schrödinger Suite<sup>85</sup>, first using Standard Precision (SP), to check quality of the model and the binding site, and then with Extra precision (XP) settings in Glide. After the first analysis of the results, docking structures were refined and structures produced in this manner were used for consideration.

The choice of protein model was governed by the following conditions: the X-ray structure has to represent an eukaryotic enzyme, taken with good resolution, with ligand bound into binding site. Also, due to our docking protocol, larger bioisosteric ligands were preferred, as that would give us binding site that can accommodate variety of ligand structures. Binding sites were prepared using previously bounded ligand. Pictures were produced using Maestro from Schrödinger Suite, or BOVIA Discovery Studio 2021 and Ligand interaction modules therein<sup>86</sup>. Data and graphical representations for representative compounds are provided in the [Supplementary material](#). Complete data and graphical representations for all compounds are available on request.

### Synthesis of the drug candidates

All chromatographic separations<sup>87</sup> were performed with silica gel, 10–18, 60 Å (dry-flash), 60 (0.063–0.200 mm; column chromatography) and ion exchange column chromatography (acidic resin DOWEX 50WX8–100). Standard techniques were used for the purification of reagents and solvents<sup>88</sup>. NMR spectra were recorded on Varian/Agilent 400 (<sup>1</sup>H NMR at 400 MHz, <sup>13</sup>C NMR at 100 MHz) and Bruker Avance III 500 (<sup>1</sup>H NMR at 500 MHz, <sup>13</sup>C NMR at 125 MHz). Chemical shifts are expressed in ppm ( $\delta$ ) using tetramethylsilane as internal standard, coupling constants (J) are in Hz. IR spectra were recorded on Thermo Scientific Nicolet Summit FT-IR instrument, and are expressed in  $\text{cm}^{-1}$ . Mass spectra were obtained on Orbitrap Exploris 240 spectrometer. Melting point was determined on LLG-unIMELT 2 melting point apparatus and is uncorrected. Optical rotation was measured on Rudolph Research Analytical AUTOPOL IV Automatic Polarimeter.

### Synthesis of $\alpha$ -glucosidase inhibitors

DNJ analogues 1, 2, 22, 75, 76, and 77 were obtained from the key intermediate 74. This compound is obtained according to the modified literature procedure<sup>58</sup>, as described in the [Supplementary material](#). Compounds 1, 2, 22, 75, 76, and 77 were obtained by alkylation (or reductive amination) of 74, followed by deprotection. Synthesis of compounds 22 (by alkylation) and 77 (by reductive amination), as well as of compound 80 is described below; for syntheses of other DNJ analogues, *i.e.*, compounds 1, 2, 75, and 76 please, see the [Supplementary material](#).

### Synthesis of the BCP fragment (80)

**A) 2-((5-(bicyclo[1.1.1]pentan-1-yl)pentyl)oxy)tetrahydro-2H-pyran (114)<sup>89</sup>.** To a solution of iodoalkane 78 (1.87 g; 6.29 mmol) and bicyclo[1.1.1]pentane 79<sup>90</sup> (0.9 M in diethyl ether; 7.50 ml; 6.75 mmol) in

anhydrous Et<sub>2</sub>O (10 ml), a solution of MeLi in diethoxymethane (3.1 M, 1.98 ml, 6.04 mmol) was added dropwise at  $-40^{\circ}\text{C}$ , under an argon atmosphere. The reaction mixture was allowed to warm to room temperature, stirred for 24 h, and then cooled again to  $-40^{\circ}\text{C}$ , when MeOH (0.1 ml) was added. The resulting solution was poured into an ice-cold mixture of H<sub>2</sub>O and pentane. After separation of the layers, the organic phase was washed with water, dried, and concentrated under reduced pressure. The crude 2-((5-(3-iodobicyclo[1.1.1]pentan-1-yl)pentyl)oxy)tetrahydro-2H-pyran (**113**, 2.29 g) was used in the next step without purification.

A deaerated solution of the iodide **113** from the previous step (2.29 g, 6.29 mmol), tributyltin hydride (2.56 g, 8.80 mmol) and AIBN (50.0 mg, 0.31 mmol) in benzene (20 ml) was stirred at  $80^{\circ}\text{C}$  under an argon atmosphere. After 1 h, a second batch of AIBN (50 mg, 0.31 mmol) was added and the reaction mixture was stirred for 1 h. After removal of the solvent under reduced pressure, the residue was purified by dry-flash chromatography (eluent: petroleum ether/ethyl acetate = 95:5) to give 2-((5-(bicyclo[1.1.1]pentan-1-yl)pentyl)oxy)tetrahydro-2H-pyran (**114**; 1.32 g, 88%) as a colourless oil. <sup>1</sup>H NMR (400 MHz, CDCl<sub>3</sub>)  $\delta$  4.59–4.55 (m, 1H), 3.90–3.84 (m, 1H), 3.76–3.69 (m, 1H), 3.53–3.47 (m, 1H), 3.40–3.35 (m, 1H), 2.43 (s, 1H), 1.88–1.78 (m, 1H), 1.74–1.68 (m, 1H), 1.67–1.47 (m, 12H), 1.40–1.24 (m, 6H). <sup>13</sup>C NMR (100 MHz, CDCl<sub>3</sub>)  $\delta$  98.9, 67.7, 62.2, 50.4, 45.9, 32.6, 30.9, 29.9, 27.4, 26.5 (2C), 25.6, 19.8. IR (ATR):  $\nu^{\sim}$  = 2961, 2927, 1460, 1281, 1194, 1048 cm<sup>-1</sup>.

**B) 5-(bicyclo[1.1.1]pentan-1-yl)pentan-1-ol (115).** To a solution of 2-((5-(bicyclo[1.1.1]pentan-1-yl)pentyl)oxy)tetrahydro-2H-pyran, **114** (1.32 g; 5.53 mmol) in methanol (20 ml) was added *p*-T<sub>5</sub>OH (47.0 mg; 0.276 mmol) and the reaction mixture was stirred at rt. After 45 min triethyl amine (3 drops) was added, the mixture was concentrated under reduced pressure and the residue was purified by dry-flash chromatography (eluent: hexane/ethyl acetate = 8:2) to give 5-(bicyclo[1.1.1]pentan-1-yl)pentan-1-ol, **115** (809 mg, 95%) as a colourless oil. <sup>1</sup>H NMR (400 MHz, CDCl<sub>3</sub>)  $\delta$  3.62 (t, *J* = 6.6 Hz, 2H), 2.44 (s, 1H), 1.63 (s, 6H), 1.57–1.52 (m, 2H), 1.40–1.24 (m, 6H). <sup>13</sup>C NMR (100 MHz, CDCl<sub>3</sub>)  $\delta$  63.0, 50.4, 45.8, 32.9, 32.7, 27.5, 26.5, 26.0. IR (ATR):  $\nu^{\sim}$  = 3331, 2960, 2929, 2867, 1461, 1280, 1194, 1054 cm<sup>-1</sup>.

**C) 1-(5-Iodopentyl)bicyclo[1.1.1]pentane (80).** To a solution of alcohol **115** (50.0 mg; 0.324 mmol), PPh<sub>3</sub> (127.5 mg; 0.486 mmol) and imidazole (66.1 mg; 0.972 mmol) in anhydrous THF (1.0 ml), iodine (123.8 mg; 0.486 mmol) was added portionwise at  $-10^{\circ}\text{C}$ , under an argon atmosphere. The cooling bath was removed and the reaction mixture was stirred for 15 min. The reaction mixture was diluted with diethyl ether, washed with saturated Na<sub>2</sub>S<sub>2</sub>O<sub>3</sub> (aq) and brine, dried over anhydrous MgSO<sub>4</sub> and concentrated under reduced pressure. The residue was dissolved in pentane, filtered through a short pad of celite and evaporated under reduced pressure to yield 75 mg (88%) of the volatile, unstable iodide **80**, which was used in the next step without further purification.

#### Compound **22**

**A) Synthesis of perbenzylated intermediate by alkylation: (2R,3R,4R,5S)-3,4,5-tris(Benzyloxy)-2-((benzyloxy)methyl)-1-(5-(bicyclo[1.1.1]pentan-1-yl)pentyl)piperidine (22A).** A solution of amine **74**<sup>58</sup> (46.2 mg; 0.088 mmol), iodide **80** (35.0 mg; 0.13 mmol) and K<sub>2</sub>CO<sub>3</sub> (42.6 mg; 0.308 mmol) in DMF (0.25 ml) was stirred at  $80^{\circ}\text{C}$  under an argon atmosphere. After 6 h, the mixture was diluted with diethyl ether, washed with H<sub>2</sub>O and saturated NaHCO<sub>3</sub>(aq), dried over anhydrous MgSO<sub>4</sub>, filtered and concentrated under reduced pressure. The crude residue was purified by column chromatography (petroleum

ether/ethyl acetate = 8:2), to afford 50.0 mg (86%) of the subtitle compound **22A** as a viscous oil.  $[\alpha]_D^{20}$   $-2.41$  (c 1.32 in CHCl<sub>3</sub>). <sup>1</sup>H NMR (500 MHz, CDCl<sub>3</sub>)  $\delta$  7.35–7.24 (m, 18H), 7.13–7.11 (m, 2H), 4.96 (d, *J* = 11.1, 1H), 4.87 (d, *J* = 10.8, 1H), 4.81 (d, *J* = 11.2, 1H), 4.69 (d, *J* = 11.9, 1H), 4.65 (d, *J* = 11.9, 1H), 4.48 (s, 1H), 4.39 (d, *J* = 10.8, 1H), 3.68–3.63 (m, 2H), 3.60 (t, *J* = 9.3, 1H), 3.52 (dd, *J*<sub>1</sub> = 10.3, *J*<sub>2</sub> = 2.0, 1H), 3.45 (t, *J* = 9.1, 1H), 3.09 (dd, *J*<sub>1</sub> = 11.1, *J*<sub>2</sub> = 4.8, 1H), 2.68–2.62 (m, 1H), 2.59–2.53 (m, 1H), 2.45 (s, 1H), 2.29 (d, *J* = 9.5, 1H), 2.23 (t, *J* = 10.8, 1H), 1.63 (s, 6H), 1.40–1.28 (m, 4H), 1.23–1.09 (m, 4H). <sup>13</sup>C NMR (125 MHz, CDCl<sub>3</sub>)  $\delta$  139.2, 138.7, 138.0, 128.6, 128.5, 128.5, 128.4, 128.0, 127.9, 127.7, 127.6, 127.5, 87.6, 78.7, 75.4, 75.3, 73.6, 72.9, 65.5 (2C), 63.9, 54.6, 52.5, 50.5, 45.9, 32.6, 27.8, 27.5, 26.6, 23.8. Under recording conditions 4 signals from Bn groups are superimposed. IR (ATR):  $\nu^{\sim}$  = 3030, 2059, 2866, 1496, 1454, 1361, 1194, 1173, 1097, 1028. cm<sup>-1</sup>. HRMS (m/z) [M-H]<sup>+</sup> calcd. for C<sub>44</sub>H<sub>54</sub>NO<sub>4</sub>: 660.4047, found: 660.4071.

**B) Deprotection into (2R,3R,4R,5S)-1-(5-(Bicyclo[1.1.1]pentan-1-yl)pentyl)-3,4,5-trihydroxy-2-(hydroxymethyl)piperidin-1-ium chloride (22).** A mixture of the compound from the previous step (50.0 mg; 0.076 mmol) and Pd(OH)<sub>2</sub> (48.0 mg) in a mixture of methanol/1 M HCl<sub>(aq)</sub> (4.0 ml, v/v = 2/1) was stirred overnight under a hydrogen atmosphere (4 atm). The mixture was filtered and concentrated under reduced pressure to afford the hydrochloride salt of **22** (25.0 mg, 98%) as colourless film.  $[\alpha]_D^{20}$   $-3.80$  (c 1.0 in H<sub>2</sub>O). <sup>1</sup>H NMR (400 MHz, D<sub>2</sub>O)  $\delta$  4.12 (d, *J* = 13.4, 1H), 3.99 (d, *J* = 13.2, 1H), 3.86–3.78 (m, 1H), 3.68 (t, *J* = 10.0, 1H), 3.62–3.52 (m, 2H), 3.43–3.37 (m, 1H), 3.27–3.18 (m, 2H), 3.11 (t, *J* = 11.8, 1H), 2.45 (s, 1H), 1.80–1.69 (m, 2H), 1.66 (s, 6H), 1.44–1.31 (m, 6H). <sup>13</sup>C NMR (100 MHz, D<sub>2</sub>O)  $\delta$  75.7, 67.0, 66.0, 65.1, 53.5, 53.1, 52.9, 49.8, 44.9, 31.4, 26.8, 25.8, 25.2, 22.1. IR (ATR):  $\nu^{\sim}$  = 3332, 2960, 2905, 2667, 1641, 1458, 1277, 1194, 1088, 1029 cm<sup>-1</sup>. HRMS (m/z) [M + H]<sup>+</sup> calcd. for C<sub>16</sub>H<sub>30</sub>NO<sub>4</sub>: 300.2169, found: 300.2178.

#### Compound **77**

**A) Synthesis of perbenzylated intermediate by reductive amination: (2R,3R,4R,5S)-1-(5-(adamantan-1-ylmethoxy)pentyl)-3,4,5-tris(benzyloxy)-2-((benzyloxy)methyl)piperidine (77A).** A solution of amine **74**<sup>58</sup> (45.0 mg; 0.086 mmol), 5-(adamantan-1-ylmethoxy)pentanal (32.0 mg; 0.128 mmol), 10% Pd/C (16 mg; 0.015 mmol) and acetic acid (0.05 ml) in ethanol (2.6 ml) was stirred overnight under a hydrogen atmosphere (4 atm). The mixture was filtered, concentrated under reduced pressure and purified by column chromatography (eluent: petroleum ether/ethyl acetate = 8:2), to afford 51.9 mg (80%) of the subtitle compound **77A**, as a colourless oil. <sup>1</sup>H NMR (400 MHz, CDCl<sub>3</sub>)  $\delta$  7.38–7.22 (m, 18H), 7.17–7.11 (m, 2H), 4.96 (d, *J* = 11.1 Hz, 1H), 4.88 (d, *J* = 10.9 Hz, 1H), 4.82 (d, *J* = 11.1 Hz, 1H), 4.73–4.62 (m, 2H), 4.53–4.44 (m, 2H), 4.43 (d, *J* = 11.0 Hz, 1H), 3.72–3.52 (m, 4H), 3.46 (t, *J* = 9.1 Hz, 1H), 3.34 (t, *J* = 6.4 Hz, 2H), 3.10 (dd, *J* = 11.1, 4.8 Hz, 1H), 2.10 (s, 1H), 2.75–2.64 (m, 1H), 2.63–2.53 (m, 1H), 2.32 (d, *J* = 9.5 Hz, 1H), 2.24 (t, *J* = 10.8 Hz, 1H), 1.97 (s, 3H), 1.76–1.62 (m, 6H), 1.57–1.12 (m, 13H). <sup>13</sup>C NMR (126 MHz, CDCl<sub>3</sub>)  $\delta$  139.0, 138.5 (2C), 137.8, 128.3 (2C), 128.2 (2C), 127.8, 127.7, 127.5, 127.4, 127.3, 87.3, 81.9, 78.5 (2C), 75.2, 75.1, 73.4, 72.7, 71.4, 65.4, 63.6, 54.4, 52.3, 39.7, 37.2, 34.1, 29.4, 28.3, 24.1, 23.3.

**B) Deprotection into (2R,3R,4R,5S)-1-(5-(adamantan-1-ylmethoxy)pentyl)-2-(hydroxymethyl)piperidine-3,4,5-triol (77)<sup>91</sup>.** A mixture of (2R,3R,4R,5S)-1-(5-(adamantan-1-ylmethoxy)pentyl)-3,4,5-tris(benzyloxy)-2-((benzyloxy)methyl)piperidine from the previous step (42.4 mg; 0.056 mmol) and Pd(OH)<sub>2</sub> (43.0 mg) in a mixture of

methanol/1 M HCl<sub>(aq)</sub> (4.8 ml, v/v = 2.7/1) was stirred overnight under a hydrogen atmosphere (4 atm). The mixture was filtered and concentrated under reduced pressure. The crude residue was purified by column chromatography (gradient ethyl acetate/methanol/25% NH<sub>3</sub> (aq) = 95:5:0.05 to 7:3:0.05) to afford 22.0 mg (100%) of the product **77** as a viscous oil. <sup>1</sup>H NMR (400 MHz, CD<sub>3</sub>OD) δ 3.96 (dd, *J* = 12.3, 1.8 Hz, 1H), 3.87 (dd, *J* = 12.3, 2.7 Hz, 1H), 3.59 (td, *J* = 10.5, 4.8 Hz, 1H), 3.47 (t, *J* = 9.5 Hz, 1H), 3.38 (t, *J* = 6.2 Hz, 2H), 3.32 (s, 1H), 3.30–3.18 (m, 2H), 3.13–3.02 (m, 1H), 2.98–2.85 (m, 3H), 2.66–2.55 (m, 2H), 1.95–1.89 (m, 3H), 1.77–1.52 (m, 15H), 1.46–1.33 (m, 2H). <sup>13</sup>C NMR (100 MHz, D<sub>2</sub>O) δ 83.1, 79.2, 72.3, 70.3, 69.1, 67.3, 57.2, 56.1, 53.9, 40.8, 38.3, 35.1, 30.3, 29.7, 24.9, 24.5.

### Synthesis of α-galactosidase inhibitors

DGJ analogues **53**, **87**, **88**, and **89** were obtained from the key intermediate **85**, by reductive amination (or alkylation), followed by deprotection. Syntheses of compounds **85**, **4**, and **88** are described below<sup>59</sup>. Syntheses of DGJ analogues, *i.e.*, compounds **53**, **87** and **89** are described in the [Supplementary material](#).

Compound **85**<sup>59</sup>

**A) Synthesis of aldol products benzyl ((2S,3S)-2-((tert-butyl-dimethylsilyloxy)-3-((R)-2,2-dimethyl-5-oxo-1,3-dioxan-4-yl)-3-hydroxypropyl)carbamate (83) and benzyl (4aS,7S,8S,8aR)-7-((tert-butyl-dimethylsilyloxy)-4a,8-dihydroxy-2,2-dimethylhexahydro-5H-[1,3]dioxino[5,4-b]pyridine-5-carboxylate (84)).** A catalytic amount of (*R*)-proline (385 mg; 3.34 mmol; 30 mol %) was added to a vial that contained benzyl (S)-2-((tert-butyl-dimethylsilyloxy)-3-oxopropyl)carbamate **81** (3.76 g; 11.15 mmol) and dioxanone **82** (2.9 g; 22.30 mmol; 2 eq) in DMF (22.5 ml). The reaction mixture was vigorously stirred at 4 °C for 96 h (during this time 3 × 1.0 g of dioxanone were added). The reaction mixture was diluted with Et<sub>2</sub>O and water. The aqueous phase was extracted twice with Et<sub>2</sub>O and the combined organic extract was washed with water, dried over anhydrous MgSO<sub>4</sub>, filtered, and concentrated under reduced pressure. The crude residue was purified by dry-flash chromatography (eluent: petroleum ether/ethyl acetate = 85:15) to furnish aldol products **83**, **84** (3.15 g; 61%), as a white foam.

**B) Deprotection into (4aR,7S,8S,8aS)-7-((tert-butyl-dimethylsilyloxy)-2,2-dimethylhexahydro-4H-[1,3]dioxino[5,4-b]pyridin-8-ol (85)).** A mixture of aldols **83**, **84** (3.15 g, 6.79 mmol) and 10% Pd/C (1.14 g, 1.07 mmol, 16 mol %) in ethanol (146 ml) was stirred for 3.5 h under a hydrogen atmosphere (4.5 atm). The mixture was filtered and concentrated under reduced pressure. Purification of the residue by dry-flash chromatography (eluent: ethyl acetate/methanol = 9:1) afforded amine **85** (1.61 g, 75%) as white crystals. [ $\alpha$ ]<sub>D</sub><sup>20</sup> +69.4 (c 0.41 in CHCl<sub>3</sub>). <sup>1</sup>H NMR (400 MHz, CHCl<sub>3</sub>) δ 4.24 (d, *J* = 2.1 Hz, 1H), 4.10 (dd, *J* = 12.0, 2.3 Hz, 1H), 3.76 (dd, *J* = 12.2, 1.3 Hz, 1H), 3.73–3.67 (m, 1H), 3.38 (dd, *J* = 9.0, 3.4 Hz, 1H), 3.09 (dd, *J* = 13.7, 5.2 Hz, 1H), 2.49 (s, 1H), 2.44 (dd, *J* = 13.7, 10.5 Hz, 1H), 2.27 (bs, 2H, OH, NH), 1.47 (s, 3H), 1.44 (s, 3H), 0.90 (s, 9H), 0.12 (s, 3H), 0.10 (s, 3H). <sup>13</sup>C NMR (100 MHz, CDCl<sub>3</sub>) δ 98.7, 75.6, 71.0, 70.4, 64.2, 51.7, 50.8, 29.8, 26.0, 18.4, 18.2, –4.3, –4.4.

**(2R,3S,4R,5S)-2-(hydroxymethyl)piperidine-3,4,5-triol (DGJ, migalastat, 4)<sup>59</sup>.** A solution of amine **85** (17.0 mg, 0.05 mmol) in solvent mixture methanol/HCl (3 M; 2.1 ml, v/v = 2:1) was stirred at room temperature for 6 h. After the volatiles were removed under

reduced pressure, the residue was purified by ion exchange chromatography (acidic resin DOWEX 50WX8–100), to give compound **4** (7.5 mg, 86%) as a colourless viscous oil. [ $\alpha$ ]<sub>D</sub><sup>20</sup> +41.4 (c 0.94 in H<sub>2</sub>O). <sup>1</sup>H NMR (500 MHz, CD<sub>3</sub>OD) δ 3.93–3.90 (m, 1H), 3.72 (td, *J* = 10.1, 5.3 Hz, 1H), 3.67–3.57 (m, 2H), 3.33–3.26 (m, 1H), 3.10 (dd, *J* = 12.5, 5.3 Hz, 1H), 2.63 (t, *J* = 6.5 Hz, 1H), 2.40–2.30 (m, 1H). <sup>13</sup>C NMR (125 MHz, CD<sub>3</sub>OD) δ 77.4, 70.8, 69.9, 63.2, 61.3, 51.5.

Compound **88**<sup>22,92</sup>

**A) Synthesis of intermediate (4aR,7S,8S,8aS)-5-butyl-7-((tert-butyl-dimethylsilyloxy)-2,2-dimethylhexahydro-4H-[1,3]dioxino[5,4-b]pyridin-8-ol (117) by reductive amination.** A mixture of amine **85**<sup>59</sup> (33.5 mg; 0.105 mmol), butanal (38.0 mg; 0.528 mmol) and 10% Pd/C (21.0 mg; 0.018 mmol) in ethanol (3.0 ml) was stirred overnight under a hydrogen atmosphere (4 atm). The mixture was filtered and concentrated under reduced pressure to afford crude **117** which was used in the next step without further purification.

**B) Deprotection into (2R,3S,4R,5S)-1-butyl-2-(hydroxymethyl)piperidine-3,4,5-triol (88).** A solution of (4aR,7S,8S,8aS)-5-butyl-7-((tert-butyl-dimethylsilyloxy)-2,2-dimethylhexahydro-4H-[1,3]dioxino[5,4-b]pyridin-8-ol, **117** (39.0 mg, 0.105 mmol) in methanol/3M HCl<sub>(aq)</sub> solvent mixture (1.6 ml, v/v = 3:1) was stirred at room temperature for 4 h. After the volatiles were removed under reduced pressure, the residue was purified by column chromatography (ethyl acetate/methanol/25% NH<sub>3</sub> (aq) = 3:2:0.05), to afford 11.4 mg (49%) of the product **88**, as a viscous oil. [ $\alpha$ ]<sub>D</sub><sup>20</sup> –21.6 (c 0.47 in MeOH). <sup>1</sup>H NMR (500 MHz, CD<sub>3</sub>OD) δ 4.01–3.99 (m, 1H), 3.85–3.81 (m, 3H), 3.25 (dd, *J* = 9.1, 3.2 Hz, 1H), 3.03 (dd, *J* = 11.4, 5.0 Hz, 1H), 2.81–2.75 (m, 1H), 2.61–2.55 (m, 1H), 2.49 (bs, 1H), 2.21 (t, *J* = 10.8 Hz, 1H), 1.54–1.47 (m, 2H), 1.35–1.27 (m, 2H), 0.95 (t, *J* = 7.3 Hz, 3H). <sup>13</sup>C NMR (125 MHz, CD<sub>3</sub>OD) δ 77.0, 72.0, 68.7, 65.3, 62.1, 57.7, 53.9, 27.1, 21.7, 14.3.

4-(–)-Epi-fagomine **93** was synthesised according to the previously published procedure<sup>60</sup>. The synthesis of the analogue **94** is described in the [Supplementary material](#).

Synthesis of pyrrolidine analogues

**Benzyl (4aS,6R,7R,7aR)-6-(((tert-butyl-dimethylsilyloxy)methyl)-4a,7-dihydroxy-2,2-dimethyltetrahydro-[1,3]dioxino[5,4-b]pyrrole-5(4H)-carboxylate (98) and benzyl ((1R,2S)-3-((tert-butyl-dimethylsilyloxy)-1-((S)-2,2-dimethyl-5-oxo-1,3-dioxan-4-yl)-1-hydroxypropan-2-yl)carbamate (99)<sup>59</sup>.** A solution of squalemic aldehyde **97** ((*R*)-**97**: (*S*)-**97** = 2:1; 1.17 g, 3.38 mmol), dioxanone (3.22 g, 70% in DMF, 17 mmol) and (*R*)-Proline (117 mg, 1 mmol, 1) in DMF (9 ml) was stirred for 48 h at 4 °C. The reaction mixture was diluted with ethyl-acetate and water. The aqueous phase was extracted three times with ethyl-acetate and the combined organic extract was washed with water, dried over anhydrous MgSO<sub>4</sub>, filtered, and concentrated under reduced pressure. The crude residue was purified by dry-flash chromatography (eluent: toluene/ethyl acetate = 4:1) to afford 605 mg (37%) of compound **98** and 533 mg (33%) of compound aldol **99**, both as viscous oil.

**Benzyl (4aS,6R,7R,7aR)-6-(((tert-butyl-dimethylsilyloxy)methyl)-4a,7-dihydroxy-2,2-dimethyltetrahydro-[1,3]dioxino[5,4-b]pyrrole-5(4H)-carboxylate (98):** <sup>1</sup>H NMR (400 MHz, DMSO-d<sub>6</sub>, 338 K) δ 7.37–7.33 (m, 5H), 5.35 (br. s, 1H), 5.12–5.05 (m, 2H), 4.47 (d, *J* = 6.88, 1H), 4.34 (dd, *J*<sub>1</sub> = 6.9, *J*<sub>2</sub> = 5.7, 1H), 3.82 (d, *J* = 5.4, 1H), 3.80 (d, *J* = 13.2, 1H), 3.72 (d, *J* = 10.5, 1H), 3.60–3.57 (m, 1H), 1.38 (s, 3H), 1.28 (s, 3H), 0.85 (s, 9H), 0.00 (s, 3H), –0.02 (s, 3H). <sup>13</sup>C



NMR (100 MHz, DMSO- $d_6$ , 338 K)  $\delta$  d 153.2, 136.4, 128.0, 127.5, 127.3, 98.4, 86.7, 75.6, 68.0, 65.6, 65.5, 64.4, 25.5, 17.6, -5.8, -5.8.

**Benzyl ((1R,2S)-3-((tert-butylidimethylsilyloxy)-1-((S)-2,2-dimethyl-5-oxo-1,3-dioxan-4-yl)-1-hydroxypropan-2-yl)carbamate (99))**:  $^1\text{H}$  NMR (400 MHz,  $\text{CDCl}_3$ )  $\delta$  7.40–7.29 (m, 5H), 5.18 (d,  $J=9.3$ , 1H), 5.12 (d,  $J=12.2$ , 1H), 5.04 (d,  $J=12.5$ , 1H), 4.29 (m, 1H), 4.17 (d,  $J=9.7$ , 1H), 4.14 (d,  $J=8.0$ , 1H), 4.06–3.99 (m, 2H), 3.73–3.66 (m, 2H), 3.50 (s, 1H), 1.39 (s, 3H), 1.33 (s, 3H), 0.88 (s, 9H), 0.06 (s, 6H).  $^{13}\text{C}$  NMR (100 MHz,  $\text{CDCl}_3$ )  $\delta$  212.6, 156.1, 136.7, 128.6, 128.3, 128.3, 101.6, 71.8, 68.6, 66.9, 66.7, 62.9, 51.4, 26.0, 23.5, 23.3, 18.4, -5.3, -5.3.

**2,5-Dideoxy-2,5-imino-D-altritol (DIA) (42)**. A mixture of amina **98** (60 mg, 0.13 mmol) and 10% Pd/C (30 mg, 0.03 mmol) in ethanol (12 ml) was stirred under a hydrogen atmosphere (4.5 bar) for 2 h. The mixture was filtered and concentrated under reduced pressure to afford crude (4aR,6R,7R,7aS)-6-(((tert-butylidimethylsilyloxy)methyl)-2,2-dimethylhexahydro-[1,3]dioxino[5,4-b]pyrrol-7-ol which was used in the next step without further purification.

A solution of crude (4aR,6R,7R,7aS)-6-(((tert-butylidimethylsilyloxy)methyl)-2,2-dimethylhexahydro-[1,3]dioxino[5,4-b]pyrrol-7-ol in solvent mixture methanol/HCl (3 M; 3.6 ml, v/v = 2:1) was stirred at room temperature for 2 h. After the volatiles were removed under reduced pressure, the residue was purified by column chromatography (1-propanol/25%  $\text{NH}_4\text{OH}$ ) and ion exchange chromatography (acidic resin DOWEX 50WX8-100) to afford 9 mg (43%) of the compound **42**, as a viscous oil.  $[\alpha]_D^{20} = +21.9$  (c 1.02 in  $\text{H}_2\text{O}$ );  $^1\text{H}$  NMR (400 MHz,  $\text{D}_2\text{O}$ )  $\delta$  4.19 (t,  $J=4.1$ , 1H), 4.00 (dd,  $J=8.5$ , 4.3 Hz, 1H), 3.80 (dd,  $J=11.1$ , 6.8 Hz, 1H), 3.75 (dd,  $J=11.8$ , 3.9 Hz, 1H), 3.68–3.62 (m, 2H), 3.35–3.30 (m, 1H), 3.17–3.11 (m, 1H).  $^{13}\text{C}$  NMR (100 MHz,  $\text{D}_2\text{O}$ )  $\delta$  73.5, 71.9, 61.8, 61.3, 60.4, 59.7.

Compound **41**

**A) Synthesis of intermediate (4aS,6R,7S,7aR)-6-(((tert-butylidimethylsilyloxy)methyl)-2,2-dimethylhexahydro-[1,3]dioxino[5,4-b]pyrrol-7-ol (99A) by reductive amination**. A mixture of aldol **99** (80 mg, 0.17 mmol) and 10% Pd/C (40 mg, 0.04 mmol) in ethanol (16 ml) was stirred under a hydrogen atmosphere (4.5 bar) for 2 h. After the volatiles were removed under reduced pressure, the residue was purified by column chromatography (dichloromethane/methanol = 95:5) to afford 40 mg (74%) of (4aS,6R,7S,7aR)-6-(((tert-butylidimethylsilyloxy)methyl)-2,2-dimethylhexahydro-[1,3]dioxino[5,4-b]pyrrol-7-ol, **99A** as colourless oil.  $^1\text{H}$  NMR (400 MHz,  $\text{CDCl}_3$ )  $\delta$  4.37–4.34 (m, 1H), 4.22 (dd,  $J=4.8$ , 3.3 Hz, 1H), 4.17 (dd,  $J=12.6$ , 3.2 Hz, 1H), 3.99 (dd,  $J=5.9$ , 4.3 Hz, 1H), 3.92 (dd,  $J=10.2$ , 3.8 Hz, 1H), 3.88–3.84 (m, 1H), 3.19 (dt,  $J=7.9$ , 3.9 Hz, 1H), 2.75–2.71 (m, 1H), 1.49 (s, 3H), 1.42 (s, 3H), 0.92 (s, 9H), 0.11 (s, 3H), 0.10 (s, 3H).  $^{13}\text{C}$  NMR (100 MHz,  $\text{CDCl}_3$ )  $\delta$  98.5, 76.3, 70.6, 62.0, 61.7, 60.7, 53.7, 29.2, 26.1, 19.4, 18.5, -5.3, -5.3. IR (ATR)  $\nu^{\sim}$  = 3555, 3290, 2991, 2953, 2930, 2885, 2857, 1471, 1426, 1380, 1255, 1228, 1198, 1171, 1125, 1081, 1023, 1006, 939, 838, 778, 713, 669. HRMS (m/z)  $[\text{M} + \text{H}]^+$  calcd. for  $\text{C}_{15}\text{H}_{32}\text{NO}_4\text{Si}$ : 318.2095; found 318.2082.

**B) Deprotection into 2,5-dideoxy-2,5-imino-D-galacticol (DMDP) (41)**. A solution of (4aS,6R,7S,7aR)-6-(((tert-butylidimethylsilyloxy)methyl)-2,2-dimethylhexahydro-[1,3]dioxino[5,4-b]pyrrol-7-ol, **99A** (40 mg, 0.13 mmol) in solvent mixture methanol/HCl (3 M; 5.4 ml, v/v = 2:1) was stirred at room temperature for 2 h. After the volatiles were removed under reduced pressure, the residue was purified by ion exchange chromatography (acidic resin DOWEX 50WX8-100) to afford 15.5 mg (75%) of the product **41**.  $^1\text{H}$  NMR (400 MHz,  $\text{D}_2\text{O}$ )  $\delta$  4.32–4.28 (m, 2H), 3.79 (dd,  $J=11.3$ , 5.6 Hz, 2H),

3.67 (dd,  $J=11.3$ , 5.6 Hz, 2H), 3.32–3.27 (m, 2H).  $^{13}\text{C}$  NMR (100 MHz,  $\text{D}_2\text{O}$ )  $\delta$  71.6, 60.3, 59.6.

Synthesis of AGF (**40**) and its methyl derivative (**104**)

**(3R,4S,5R)-3-(hydroxymethyl)hexahydropyridazine-4,5-diol hydrochloride (AGF, 40)**. A solution of amine **102** (20.0 mg, 0.069 mmol) in a solvent mixture methanol/HCl (6 M; 0.6 ml, v/v = 1:1) was stirred at room temperature overnight. Volatiles were removed under reduced pressure to give compound **40** (12.5 mg, 98%), as a colourless viscous oil.  $^1\text{H}$  NMR (500 MHz,  $\text{D}_2\text{O}$ )  $\delta$  4.07–4.04 (m, 1H), 3.95 (ddd,  $J=11.3$ , 5.2, 2.8 Hz, 1H), 3.75 (dd,  $J=13.7$ , 6.6 Hz, 1H), 3.35–2.30 (m, 1H), 3.25 (dd,  $J=12.7$ , 5.1 Hz, 1H), 3.19–3.11 (m, 1H).  $^{13}\text{C}$  NMR (125 MHz,  $\text{D}_2\text{O}$ )  $\delta$  65.0, 64.8, 60.4, 59.5, 44.0. IR (ATR)  $\nu^{\sim}$  = 3274, 2932, 1570, 1413, 1102, 1029, 817, 657  $\text{cm}^{-1}$ .

**tert-Butyl (4R,4aS,8aR)-4-hydroxy-6,6-dimethyltetrahydro-1H-[1,3]dioxino[5,4-c]pyridazine-2(3H)-carboxylate (102)<sup>61</sup>**. A mixture of aldol **101**<sup>61</sup> (500.0 mg; 1.140 mmol) and 10% Pd/C (100.0 mg; 0.094 mmol) in methanol (30.0 ml) was stirred under a hydrogen atmosphere (1 atm) for 1 h. The mixture was filtered through a short pad of celite and evaporated under reduced pressure to afford the crude product, which was used in the next step without further purification.

The crude product from the previous step was dissolved in methanol (2.0 ml) and acetic acid (8.0 ml) was added to the solution. After 2 min, sodium cyanoborohydride (215.0 mg; 3.421 mmol) was added and the mixture was stirred for 30 min at room temperature. After reaction completion, the mixture was diluted with dichloromethane and washed with  $\text{H}_2\text{O}$ , saturated  $\text{NaHCO}_3(\text{aq})$  and brine. Organic layer was dried over anhydrous  $\text{MgSO}_4$  and volatiles were removed under reduced pressure. The residue was purified by dry-flash chromatography (ethyl acetate/petroleum ether/methanol = 76:20:4), to afford 212.7 mg (65%) of the product **102**, as a white solid. mp 180–181 °C.  $[\alpha]_D^{20} = +50.9$  (c 1.20, MeOH).  $^1\text{H}$  NMR (500 MHz, DMSO- $d_6$ , 65 °C)  $\delta$  4.59 (d,  $J=5.7$  Hz, 1H), 4.23 (d,  $J=11.4$  Hz, 1H), 4.07–4.00 (m, 2H), 3.81 (dd,  $J=12.2$ , 5.2 Hz, 1H), 3.60 (dd,  $J=12.3$ , 1.6 Hz, 1H), 3.49–3.42 (m, 1H), 2.90 (t,  $J=11.7$  Hz, 1H), 2.54–2.50 (m, 1H), 1.41 (s, 3H), 1.40 (s, 9H), 1.35 (s, 3H).  $^{13}\text{C}$  NMR (125 MHz, DMSO- $d_6$ , 65 °C)  $\delta$  154.4, 97.9, 78.5, 66.5, 65.8, 61.3, 51.3, 45.0, 28.9, 27.8, 18.5. IR (ATR)  $\nu^{\sim}$  = 3417, 3250, 2983, 2973, 1695, 1502, 1385, 1177, 1066, 993, 853  $\text{cm}^{-1}$ . HRMS (m/z)  $[\text{M} + \text{Na}]^+$  calcd. for  $\text{C}_{13}\text{H}_{24}\text{N}_2\text{NaO}_5$ : 311.1577; found: 311.1584

**tert-Butyl (4R,4aS,8aR)-4-hydroxy-1,6,6-trimethyltetrahydro-1H-[1,3]dioxino[5,4-c]pyridazine-2(3H)-carboxylate (103)**. A mixture of **102**<sup>61</sup> (10.0 mg; 0.035 mmol), 30% formaldehyde solution in water (19  $\mu\text{L}$ ; 0.208 mmol), 10% Pd(OH)<sub>2</sub>/C (10.0 mg; 0.009 mmol), ethyl acetate (300  $\mu\text{L}$ ) and catalytic amount of acetic acid was stirred under a hydrogen atmosphere (1 atm) for 6 h. The mixture was diluted with ethyl acetate and filtered through a short pad of celite, and volatiles were evaporated under reduced pressure. The residue was purified by column chromatography (petroleum ether/ethyl acetate = 1:2), to afford 8.8 mg (84%) of the product **103**.  $^1\text{H}$  NMR (400 MHz,  $\text{CDCl}_3$ )  $\delta$  4.09 (m, 1H), 4.05 (d,  $J=3.4$  Hz, 1H), 4.03–3.95 (m, 1H), 3.93–3.80 (m, 1H), 3.65 (m, 1H), 3.15 (bt,  $J=11.8$  Hz, 1H), 2.84 (bs, 4H), 2.51 (d,  $J=10.6$  Hz, OH), 1.48 (s, 3H), 1.45 (s, 9H), 1.42 (s, 3H).  $^{13}\text{C}$  NMR (100 MHz,  $\text{CDCl}_3$ )  $\delta$  155.4, 99.4, 80.4, 67.1, 66.4, 61.7, 53.9, 39.6, 29.5, 28.4, 18.9.

**(4R,5S,6R)-6-(hydroxymethyl)-1-methylhexahydropyridazine-4,5-diol hydrochloride (104)**. To a solution of **103** (8.3 mg; 0.027 mmol) in methanol (300  $\mu\text{L}$ ) a 3 M  $\text{HCl}(\text{aq})$  (300  $\mu\text{L}$ ) was added dropwise

and the resulting mixture was stirred for 24 h at room temperature. Volatiles were removed under reduced pressure resulting in 5.4 mg (100%) of pure product **104**.  $^1\text{H}$  NMR (400 MHz,  $\text{D}_2\text{O}$ )  $\delta$  4.28 (m, 1H), 3.98 (d,  $J=4.9$  Hz, 2H), 3.98–3.93 (m, 1H), 3.39–3.28 (m, 2H), 3.21 (dd,  $J=13.2, 5.2$  Hz, 1H), 3.04 (s, 3H).  $^{13}\text{C}$  NMR (100 MHz,  $\text{CDCl}_3$ )  $\delta$  68.1, 67.1, 65.0, 59.6, 44.5, 41.6. HRMS ( $m/z$ )  $[\text{M} + \text{H}]^+$  calcd. for  $\text{C}_6\text{H}_{14}\text{N}_2\text{O}_3$ : 163.1077; found: 163.1171.

### Synthesis of mannosidase inhibitors

(–)-Swainsonine (**3**) was synthesised according to the recently published procedure<sup>63</sup>. Compound AR524 (**71**) was obtained according to the previously published procedure<sup>55</sup>.

Experimental procedures, spectral data and copies of  $^1\text{H}$  and  $^{13}\text{C}$  NMR spectra are provided in the [Supplementary material](#).

### Enzyme assays

All chemicals were of analytical grade or higher and were purchased from Sigma-Aldrich Chemie GmbH (Taufkirchen, Germany), Torlak (Belgrade, Serbia) and Centrohem (Stara Pazova, Serbia). The synthetic gene for  $\alpha$ -glucosidase pET-22b(+) was purchased from Integrated DNA Technologies (Iowa, USA). Empty pET-22b(+) vector (Merck No: 69744–3) and *Escherichia coli* (*E. coli*) cells BL21 (DE3) strain (Novagen 69450–3) were kindly provided by Professor Dr. Stefan Schillberg, Fraunhofer-Institute, Aachen, Germany. Recombinant human  $\alpha$ -galactosidase (PDB ID: 1R46) was purchased from R&D Systems (Minneapolis, USA).

*Expression of recombinant  $\alpha$ -glucosidase* (Uniprot: P53341, MAL12\_YEAST weblink: <https://www.uniprot.org/uniprotkb/P53341/entry#structure>) in *Escherichia coli* and purification of the enzyme were performed according to modified literature procedures<sup>65</sup>. A synthetic gene encoding  $\alpha$ -glucosidase from *Saccharomyces cerevisiae* was inserted into pET-22b(+) vector to produce recombinant protein in cytosol of *Escherichia coli*. Competent *E. coli* cells, BL21 (DE3) strain, were transformed with  $\alpha$ -glucosidase-pET-22b(+) construct and vector pET-22b(+) without insert using standard heat-shock protocol. The vector without insert was used as a control of protein expression. Competent cells of *E. coli* BL21 (DE3) strain stored at  $-80^\circ\text{C}$  were thawed on ice. pET-22b(+) plasmid containing a gene and pET-22b(+) vector were mixed with competent cells, incubated on ice for 30 min, and used for heat shock treatment at  $42^\circ\text{C}$  for 45 s. After heat shock the cells were incubated on ice for 2 min followed by incubation in SOC medium (0.5% yeast extract, 2% tryptone, 10 mM NaCl, 2.5 mM KCl, 10 mM  $\text{MgCl}_2$ , 10 mM  $\text{MgSO}_4$ , 20 mM glucose). The cells were finally incubated at  $37^\circ\text{C}$  for 1 h in incubator with shaking. The cultures were centrifuged at 13000 rpm and 100  $\mu\text{l}$  of cultures were plated on sterile Luria broth (LB) solid plates with ampicillin (final concentration 100 mg/L) and left overnight. The *E. coli* transformed cells were picked from LB plates and inoculated into sterile LB liquid medium with ampicillin (final 100 mg/L). Cells were incubated at  $37^\circ\text{C}$ , 200 rpm overnight in the Biosan Orbital Shaker-Incubator ES-20.  $\beta$ -D-1-Thiogalactopyranoside (IPTG) in final concentration 0.4 mM was added when cell density expressed as  $A^{600}$  reached 0.6 and the culture was further incubated for 18 h at  $27^\circ\text{C}$ .

Recombinant enzyme produced by *E. coli* was harvested 18 h after induction. The culture was centrifuged in Beckman Centrifuge J-6M (30 min, 3000 rpm,  $4^\circ\text{C}$ ) and the collected cells were resuspended in lysis buffer (50 mM sodium phosphate, pH 7.0, 300 mM sodium chloride, 10 mM imidazole). Cells containing enzyme of interest were lysed by sonication (10 times for 10 s

with 30 s breaks) on ice. The cell lysate was centrifuged for 30 min at 13400 rpm and the supernatant was filtered through 0.22  $\mu\text{m}$  sterile filter. HisTrap fast flow Ni-NTA 5 ml column was equilibrated on a HPLC system with 25 ml of 50 mM sodium phosphate, pH 7.0 buffer (supplemented with 300 mM sodium chloride and 10 mM imidazole). Afterwards, concentrated supernatant containing  $\alpha$ -glucosidase was loaded to the column. The column was washed with 25 ml of the same buffer. Proteins were eluted using linear gradient 10–500 mM imidazole in the same buffer. Fractions with  $\alpha$ -glucosidase activity were analysed by SDS gel electrophoresis. Pooled fractions were dialysed against 20 mM sodium phosphate buffer, pH 7.0 with 10% glycerol and 1 mM DTT. The protein was of satisfactory purity. Electrophoregram showed the presence of a band of the correct molecular mass, about 65 kDa (Figure S-25).

*Inhibition of  $\alpha$ -glucosidase* by iminosugars was assayed by measuring hydrolysis rate of *p*-nitrophenyl glucoside, using modified literature procedure<sup>67a</sup>. The purified enzyme was used for inhibition assays. The enzyme assay was conducted in 96-well microtiter plate by measuring the quantity of *p*-nitrophenol released from the substrate *p*-nitrophenyl  $\alpha$ -D-glucopyranoside (pNPG) spectrophotometrically on a LKB 5060–006 Microplate Reader. Purified  $\alpha$ -glucosidase (2.5  $\mu\text{g}/\text{mL}$ ) was incubated with tested inhibitors at various concentrations (0–0.5 mM) in 100 mM sodium phosphate buffer pH 7.0 for 30 min at  $37^\circ\text{C}$  (Biosan PST-60H, Plate Shaker-Thermostat), and then pNPG (1.2 mM) was added ( $\epsilon_{\text{pNP}} = 8.3 \text{ mM}^{-1}\text{cm}^{-1}$  at 405 nm) and the absorbance change was followed at 405 nm for 25 min. All measurements were done in triplicates. Percentage of inhibition was calculated from the residual activity in comparison to the the control sample. The linear regression analysis was performed using GraphPad linear regression calculator.<sup>67b</sup> The results are shown in [Figure 8](#) and [Figures S26–S31](#).

*Inhibition of  $\alpha$ -galactosidase A* (PDB ID: 1R46) by iminosugars was assayed by measuring hydrolysis rate of *p*-nitrophenyl galactoside, using modified literature procedure.<sup>67c</sup> Recombinant human  $\alpha$ -galactosidase A was purchased from R&D Systems (Minneapolis, USA). The enzyme assay was conducted in 96-well microtiter plate by measuring the quantity of *p*-nitrophenol released from the substrate *p*-nitrophenyl  $\alpha$ -D-galactopyranoside by the commercial  $\alpha$ -galactosidase A. Increase in the absorbance at 405 nm was monitored for 90 min spectrophotometrically on a LKB 5060–006 Microplate Reader. The enzyme (0.1  $\mu\text{g}/\mu\text{L}$ ) was incubated with tested inhibitors at different concentrations (0.1–100  $\mu\text{M}$ ) in 100 mM citrate-phosphate buffer pH 4.5 for 30 min at  $37^\circ\text{C}$  (Biosan PST-60H, Plate Shaker-Thermostat). Substrate *p*-nitrophenyl  $\alpha$ -D-galactopyranoside (4 mM) was added at the end of enzyme–inhibitor incubation. Reaction aliquotes were taken during 90 min, mixed with 0.4 M sodium carbonate solution and the absorbance was measured at 405 nm. All measurements were done in triplicates. Percentage of inhibition was calculated from the residual activity in comparison to the control sample. The linear regression analysis was performed using GraphPad linear regression calculator.<sup>67b</sup> The results are shown in [Figure 9](#) and [Figures S32–S41](#).

### In vitro assays

#### Cells and viruses

African green monkey kidney epithelial cell line Vero C1008 (RRID:CVCL\_0574, ATCC CRL-1586) and Human lung epithelial cell line A549-ACE2 (RRID:CVCL\_COQ5, ATCC #CCL-185; these cells were transduced by a lentiviral construction in order to stably

express the ACE2 receptor, and were kindly provided by the lab of dr. Olivier Schwartz, Virus and Immunity Unit, Institut Pasteur, Université Paris Cité, CNRS UMR3569, Paris, France; Vaccine Research Institute, Créteil, France), were cultured in DMEM (Gibco #31966021) supplemented with 10% FBS (Gibco #A3160801) and penicillin/streptomycin (100 U/mL and 100 µg/mL, Gibco #15140122) at 37 °C in a 5% CO<sub>2</sub> atmosphere. In order to maintain the selection of the ACE2 clones, Blastidicin (10 µg/mL – Sigma Aldrich #SBR00022-10ML) was added to the media.

SARS-CoV-2 BA.1 strain (GISAID ID: EPI\_ISL\_6794907) was kindly provided by the Virus and Immunity Unit (Institut Pasteur, PMID: 35322239). Viral stocks were generated by infecting Vero C1008 cells at a multiplicity of infection (MOI) of 0.01 in DMEM supplemented with 2% of FBS and 1 µg/mL of TPCK-Trypsin (Sigma-Aldrich #1426-100MG). Supernatant was harvested 3 days post-infection (p.i.) and stored at –80 °C.

All experiments involving live SARS-CoV-2 were performed at the Institut Pasteur Paris (IPP) in compliance with IPP's guidelines following Biosafety Level 3 (BSL-3) containment procedures for airborne viruses. All experiments were performed in at least three biologically independent samples.

### Antiviral activity assays

A549-ACE2 cells were seeded in 96 well plates at a concentration of 1.5E4 cells per well in DMEM supplemented with 10% of FBS and incubated overnight at 37 °C, 5% CO<sub>2</sub>.

Two hours prior to infection, the supernatant was replaced with 100 µL of DMEM – 2% FBS containing the compound of interest at the indicated concentration (100 µM, 50 µM, 20 µM, 10 µM, 1 µM or 0.1 µM); or an equivalent volume of DMSO (Sigma Aldrich - #D2650), vehicle used as a control. At the time of infection, the media was replaced with virus inoculum (MOI = 0.1 PFU/cell).

Following a one-hour adsorption at 37 °C, the virus inoculum was replaced by 200 µL of drug- (or vehicle-) containing media and cells were incubated for an additional 72 h at 37 °C, 5% CO<sub>2</sub>. The supernatants were then collected for RT-qPCR and cell viability assay.

### Virus quantification by RT-qPCR

72 hpi, supernatants were collected and inactivated 10 min at 95 °C to further be used for RT-qPCR. SARS-CoV-2 specific primers targeting the N gene region: 5'TAATCAGACAAGGAAGTATTA-3' (Forward) and 5'CGAAGGTGTGACTTCCATG-3' (Reverse) were used with the Luna Universal One-Step RT-qPCR kit (New England Biolabs, #E3005) in an Applied Biosystems QuantStudio 6 thermocycler with the following cycling conditions: 55 °C for 10 min, 95 °C for 1 min, and 40 cycles of 95 °C for 10 s followed by 60 °C for 1 min. The number of viral genomes is expressed as PFU equivalents/mL and calculated by performing a standard curve with RNA derived from a viral stock with a known viral titre. Data were fit using nonlinear regression, and IC<sub>50</sub>s for each experiment were determined using GraphPad Prism version 8.1.0 (San Diego, CA).

### Cell toxicity assay

Cell viability was assessed in drug-treated cells by using Cell TiterGlo following the manufacturer's instructions (Promega #G7570). Luminescence was measured in a Tecan Infinity 2000 plate reader.

Percentage of viability was calculated relative to untreated cells and cells lysed with 20% of ethanol.

The numeric data for the antiviral assays and cytotoxicity assays, as well as the graphical presentation of the obtained results are provided in the [Supplementary material](#).

Supplemental information is available at [Supplementary material](#)

### Acknowledgments:

This research was supported by the Science Fund of the Republic of Serbia, within the Special Research Program COVID-19, Project No: 7547552, Acronym: SMART Repurposing.

### Author contributions statement

Zorana Ferjancic: investigation, project administration, methodology. Filip Bihelovic: investigation, project administration, methodology. Bojan Vulovic: investigation, methodology, visualisation. Radomir Matovic: investigation. Milena Trmcic: investigation, writing – review and editing. Aleksandar Jankovic: investigation. Milos Pavlovic: investigation. Filip Djurkovic: investigation. Radivoje Prodanovic: methodology, supervision, formal analysis. Aleksandra Djurdjevic Djelmas: investigation, formal analysis. Nevena Kalicanin: investigation, formal analysis. Mario Zlatovic: investigation, methodology, software, formal analysis, visualisation, data curation. Dusan Sladic: methodology, conceptualisation, supervision, formal analysis, validation, writing – original draft, writing – review & editing. Thomas Vallet: investigation, formal analysis, visualisation, methodology. Marco Vignuzzi: supervision, methodology, resources, writing – editing & review. Radomir N. Saicic: conceptualisation, funding acquisition, project administration, methodology, supervision, validation, writing – original draft, writing – editing and review.

### Declaration of interest statement

The authors report there are no competing interests to declare.

### References

1. De Clercq E, Li G. Approved antiviral drugs over the past 50 years. *Clin Microbiol Rev.* 2016;29(3):695–747.
2. Chaudhuri S, Symons JA, Deval J. Innovation and trends in the development and approval of antiviral medicines: 1987–2017 and beyond. *Antiviral Res.* 2018;155:76–88.
3. Pushpakom S, Iorio F, Eyers PA, Escott KJ, Hopper S, Wells A, Doig A, Guillemins T, Latimer J, McNamee C, et al. Drug repurposing: progress, challenges and recommendations: a review article on drug repurposing. *Nat Rev Drug Discov.* 2019;18(1):41–58.
4. a) Dotolo S, Marabotti A, Facchiano A, Tagliaferri R. A review on drug repurposing applicable to COVID-19. *Brief Bioinform.* 2021;22(2):726–741. b) Singh TU, Parida S, Lingaraju MC, Kesavan M, Kumar D, Singh RK. Drug repurposing approach to fight COVID-19. *Pharmacol Rep.* 2020; 72(6):1479–1508. c) Parvathaneni V, Gupta V. Utilizing drug repurposing against COVID-19 – efficacy, limitations, and challenges. *Life Sci.* 2020;259:118275. d) De Savi C, Hughes DL, Kvaerno L. Quest for a COVID-19 cure by repurposing small-molecule drugs: mechanism of action, clinical development, synthesis at scale, and outlook for supply. *Org Process Res Dev.* 2020;24(6):940–976.

5. a) Riva L, Yuan S, Yin X, Martin-Sancho L, Matsunaga N, Pache L, Burgstaller-Muehlbacher S, De Jesus PD, Teriete P, Hull MV, et al. Discovery of SARS-CoV-2 antiviral drugs through large-scale compound repurposing. *Nature*. 2020; 586(7827):113–119. b) Arshad U, Pertinez H, Box H, et al. Prioritization of anti-SARS-Cov-2 drug repurposing opportunities based on plasma and target site concentrations derived from their established human pharmacokinetics. *Clin Pharmacol Ther*. 2020;108(4):775–790.
6. WHO Solidarity Trial Consortium. Remdesivir and three other drugs for hospitalised patients with COVID-19: final results of the WHO Solidarity randomised trial and updated meta-analyses. *Lancet*. 2022;399(10339):1941–1953.
7. a) Al-Muhsen S, Al-Numair NS, Saheb Sharif-Askari N, Basamh R, Alyounes B, Jabaan A, Saheb Sharif-Askari F, Alosaimi MF, Alshome F, Halwani R, et al. Favipiravir effectiveness and safety in hospitalized moderate-severe COVID-19 patients: observational prospective multicenter investigation in Saudi Arabia. *Front Med (Lausanne)*. 2022;9:826247. b) McMahon JH, Lau JSY, Coldham A, Roney J, Hagenauer M, Price S, Bryant M, Garlick J, Paterson A, Lee SJ, et al. Favipiravir in early symptomatic COVID-19, a randomised placebo-controlled trial. *EClinicalMedicine*. 2022;54:101703.
8. Horby P, Lim WS, Emberson JR, Mafham M, Bell JL, Linsell L, Staplin N, Brightling C, Ustianowski A, Elmahi E, RECOVERY Collaborative Group, et al. Dexamethasone in hospitalized patients with COVID-19. *N Engl J Med*. 2021;384(8):693–704.
9. Owen DR, Allerton CMN, Anderson AS, Aschenbrenner L, Avery M, Berritt S, Boras B, Cardin RD, Carlo A, Coffman KJ, et al. An oral SARS-CoV-2 M<sup>pro</sup> inhibitor clinical candidate for the treatment of COVID-19. *Science*. 2021;374(6575): 1586–1593.
10. Kabinger F, Stiller C, Schmitzová J, Dienemann C, Kocic G, Hillen HS, Höbartner C, Cramer P. Mechanism of molnupiravir-induced SARS-CoV-2 mutagenesis. *Nat Struct Mol Biol*. 2021;28(9):740–746.
11. Moghadasi SA, Heilmann E, Khalil AM, Nnabuife C, Kearns FL, Ye C, Moraes SN, Costacurta F, Esler MA, Aihara H, et al. Transmissible SARS-CoV-2 variants with resistance to clinical protease inhibitors. *Sci Adv*. 2023;9(13):eade8778.
12. a) Dwek RA, Butters TD, Platt FM, Zitzmann N. Targeting glycosylation as a therapeutic approach. *Nat Rev Drug Discov*. 2002;1(1):65–75. b) Alonzi DS, Scott KA, Dwek RA, Zitzmann N. Iminosugar antivirals: the therapeutic sweet spot. *Biochem Soc Trans*. 2017;45(2):571–582. c) Norton PA, Gu B, Block TM. Iminosugars as antiviral agents. In: Compain P, Martin OR, editors. *Iminosugars: from synthesis to therapeutic applications*. Chichester, UK: John Wiley & Sons, Ltd; 2007. p. 209–224.
13. Tharappel AM, Samrat SK, Li Z, Li H. Targeting crucial host factors of SARS-CoV-2. *ACS Infect Dis*. 2020;6(11):2844–2865.
14. Chang J, Warren TK, Zhao X, Gill T, Guo F, Wang L, Comunale MA, Du Y, Alonzi DS, Yu W, et al. Small molecule inhibitors of ER  $\alpha$ -glucosidases are active against multiple hemorrhagic fever viruses. *Antiviral Res*. 2013;98(3):432–440.
15. Warfield KL, Alonzi DS, Hill JC, Caputo AT, Roversi P, Kiappes JL, Sheets N, Duchars M, Dwek RA, Biggins J, et al. Targeting endoplasmic reticulum  $\alpha$ -glucosidase I with a single-dose iminosugar treatment protects against lethal influenza and dengue virus infections. *J Med Chem*. 2020;63(8):4205–4214.
16. Zhao X, Guo F, Comunale MA, Mehta A, Sehgal M, Jain P, Cuconati A, Lin H, Block TM, Chang J, et al. Inhibition of endoplasmic reticulum-resident glucosidases impairs severe acute respiratory syndrome coronavirus and human coronavirus NL63 spike protein-mediated entry by altering the glycan processing of angiotensin I-converting enzyme 2. *Antimicrob Agents Chemother*. 2015;59(1):206–216.
17. Williams SJ, Goddard-Borger ED.  $\alpha$ -glucosidase inhibitors as host-directed antiviral agents with potential for the treatment of COVID-19. *Biochem Soc Trans*. 2020;48(3):1287–1295.
18. Dwek RA, Bell JI, Feldmann M, Zitzmann N. Host-targeting oral antiviral drugs to prevent pandemics. *Lancet*. 2022; 399(10333):1381–1382.
19. Chang J, Block TM, Guo J-T. Antiviral therapies targeting host ER alpha-glucosidases: current status and future directions. *Antiviral Res*. 2013;99(3):251–260.
20. a) Lyseng-Williamson KA. Miglustat: a review of its use in Niemann-Pick disease type C. *Drugs*. 2014;74(1):61–74. b) Patterson MC, Vecchio D, Prady H. Miglustat for treatment of Niemann-Pick C disease: a randomised controlled study. *Lancet Neurol*. 2007;6(9):765–772.
21. Ficiocioglu C. Review of miglustat for clinical management in Gaucher disease type 1. *Ther Clin Risk Manag*. 2008;4(2): 425–431.
22. Lahav D, Liu B, van den Berg RJBHN, van den Nieuwendijk AMCH, Wennekes T, Ghisaidoobe AT, Breen I, Ferraz MJ, Kuo C-L, Wu L, et al. A fluorescence polarization activity-based protein profiling assay in the discovery of potent, selective inhibitors for human nonlysosomal glucosylceramidase. *J Am Chem Soc*. 2017;139(40):14192–14197.
23. Sayce AC, Alonzi DS, Killingbeck SS, Tyrrell BE, Hill ML, Caputo AT, Iwaki R, Kinami K, Ide D, Kiappes JL, et al. Iminosugars inhibit dengue virus production via inhibition of ER alpha-glucosidases—not glycolipid processing enzymes. *PLoS Negl Trop Dis*. 2016;10(3):e0004524.
24. Flanagan JJ, Rossi B, Tang K, Wu X, Mascioli K, Donaudy F, Tuzzi MR, Fontana F, Cubellis MV, Porto C, et al. The pharmacological chaperone 1-deoxynojirimycin increases the activity and lysosomal trafficking of multiple mutant forms of acid alpha-glucosidase. *Hum Mutat*. 2009;30(12): 1683–1692.
25. a) Elbein AD. Glycosidase inhibitors: inhibitors of N-linked oligosaccharide processing. *Faseb J*. 1991;5(15):3055–3063. b) Tulsiani DR, Harris TM, Touster O. Swainsonine inhibits the biosynthesis of complex glycoproteins by inhibition of golgi mannosidase II. *J Biol Chem*. 1982;257(14):7936–7939.
26. a) Goss PE, Baptiste J, Fernandes B, Baker M, Dennis JW. A phase I study of swainsonine in patients with advanced malignancies. *Cancer Res*. 1994;54(6):1450–1457. b) Goss PE, Reid CL, Bailey D, et al. Phase IB clinical trial of the oligosaccharide processing inhibitor swainsonine in patients with advanced malignancies. *Clin Cancer Res*. 1997;3(7): 1077–1086. c) Shaheen PE, Stadler W, Elson P, Knox J, Winquist E, Bukowski RM. Phase II study of the efficacy and safety of oral GD0039 in patients with locally advanced or metastatic renal cell carcinoma. *Invest New Drugs*. 2005; 23(6):577–581.
27. Gordon DE, Jang GM, Bouhaddou M, Xu J, Obernier K, White KM, O'Meara MJ, Rezelj VV, Guo JZ, Swaney DL, et al. A SARS-CoV-2 protein interaction map reveals targets for drug repurposing. *Nature*. 2020;583(7816):459–468.
28. a) Pavlović D, Neville DCA, Argaud O, Blumberg B, Dwek RA, Fischer WB, Zitzmann N. The hepatitis C virus p7 protein forms an ion channel that is inhibited by long-alkyl-chain iminosugar derivatives. *Proc Natl Acad Sci USA*. 2003;

- 100(10):6104–6108. b) Durantel D, Branza-Nichita N, Carrouée-Durantel S, Butters TD, Dwek RA, Zitzmann N. Study of the mechanism of antiviral action of iminosugar derivatives against bovine viral diarrhoea virus. *J Virol*. 2001; 75(19):8987–8998.
29. a) McCafferty EH, Scott LJ. Migalastat: a review in Fabry disease. *Drugs*. 2019;79(5):543–554. b) McCafferty EH, Scott LJ. Correction to: Migalastat: a review in Fabry disease. *Drugs*. 2019;79(5):543–554.
30. Mahoney R, Lee GK, Zepeda JP, et al. Severe manifestations and treatment of COVID-19 in a transplanted patient with Fabry disease. *Mol Genet Metab Rep*. 2021;29:100802.
31. Han N, Hwang W, Tzelepis K, Schmerer P, Yankova E, MacMahon M, Lei W, M Katritsis N, Liu A, Felgenhauer U, et al. Identification of SARS-CoV-2-induced pathways reveals drug repurposing strategies. *Sci Adv*. 2021;7(27):eabh3032.
32. Caputo AT, Alonzi DS, Marti L, Reza I-B, Kiappes JL, Struwe WB, Cross A, Basu S, Lowe ED, Darlot B, et al. Structures of mammalian ER  $\alpha$ -glucosidase II capture the binding modes of broad-spectrum iminosugar antivirals. *Proc Natl Acad Sci USA*. 2016;113(32):E4630–8.
33. a) O’Keefe S, Roebuck QP, Nakagome I, Hirono S, Kato A, Nash R, High S. Characterizing the selectivity of ER  $\alpha$ -glucosidase inhibitors. *Glycobiology*. 2019;29(7):530–542. b) Satoh T, Toshimori T, Yan G, et al. Structural basis for two-step glucose trimming by glucosidase II involved in ER glycoprotein quality control. *Sci Rep*. 2016;6(1):20575.
34. Satoh T, Toshimori T, Yan G, et al. 5DL0 Crystal structure of glucosidase II alpha subunit (Glc1Man2-bound form). [Internet]. RCSB PDB. 2016; Available from: [rcsb.org/structure/5DL0](https://rcsb.org/structure/5DL0).
35. RCSB Protein Data Bank [Internet]. Available from: [rcsb.org](https://rcsb.org). (last accessed 22 December 2022).
36. Du Y, Ye H, Gill T, Wang L, Guo F, Cuconati A, Guo J-T, Block TM, Chang J, Xu X, et al. N-Alkyldeoxyjirimycin derivatives with novel terminal tertiary amide substitution for treatment of bovine viral diarrhoea virus (BVDV), Dengue, and Tacaribe virus infections. *Bioorg Med Chem Lett*. 2013;23(7):2172–2176.
37. Prell E, Korb C, Kluge R, Ströhl D, Csuk R. Amplification of the inhibitory activity and reversal of the selectivity of miglitol by C(2’)-monofluorination. *Arch Pharm (Weinheim)*. 2010;343(10):583–589.
38. De Crescenzo GA, Getman DP. 1,4-Dideoxy-4-fluoronojirimycin. *Eur. Pat. Appl.* EP481950 A2; 1992.
39. Hentges A, Bause E. Affinity purification and characterization of glucosidase II from pig liver. *Biol Chem*. 1997;378(9):1031–1038.
40. Andersen SM, Ebner M, Ekhart CW, Gradnig G, Legler G, Lundt I, Stütz AE, Withers SG, Wrodnigg T. Two isosteric fluorinated derivatives of the powerful glucosidase inhibitors, 1-deoxynojirimycin and 2,5-dideoxy-2,5-imino-d-mannitol: syntheses and glucosidase-inhibitory activities of 1,2,5-trideoxy-2-fluoro-1,5-imino-d-glucitol and of 1,2,5-trideoxy-1-fluoro-2,5-imino-d-mannitol. *Carbohydr Res*. 1997;301(3-4):155–166.
41. Berger A, Dax K, Gradnig G, Grassberger V, Stütz AE, Ungerank M, Legler G, Bause E. Synthesis and biological activity of C-6 modified derivatives of the glucosidase inhibitor 1-deoxynojirimycin. *Bioorg Med Chem Lett*. 1992;2(1):27–32.
42. Tarko L, Hirtopceanu A. QSAR study regarding the inhibitory activity of some iminosugars against  $\alpha$ -glucosidase. *Rev Chim*. 2016;67(1):13–16.
43. Ma J, Wu S, Zhang X, Guo F, Yang K, Guo J, Su Q, Lu H, Lam P, Li Y, et al. Ester Prodrugs of IHVR-19029 with enhanced oral exposure and prevention of gastrointestinal glucosidase interaction. *ACS Med Chem Lett*. 2017;8(2):157–162.
44. Kiappes JL, Hill ML, Alonzi DS, Miller JL, Iwaki R, Sayce AC, Caputo AT, Kato A, Zitzmann N. ToP-DNJ, a selective inhibitor of endoplasmic reticulum  $\alpha$ -glucosidase II exhibiting anti-flaviviral activity. *ACS Chem Biol*. 2018;13(1):60–65.
45. Cendret V, Legigan T, Mingot A, Thibaudeau S, Adachi I, Forcella M, Parenti P, Bertrand J, Becq F, Norez C, et al. Synthetic deoxynojirimycin derivatives bearing a thiolated, fluorinated or unsaturated N-alkyl chain: identification of potent  $\alpha$ -glucosidase and trehalase inhibitors as well as F508del-CFTR correctors. *Org Biomol Chem*. 2015;13(43):10734–10744.
46. Zamoner LOB, Aragão-Leoneti V, Carvalho I. Iminosugars: Effects of stereochemistry, ring size, and N-substituents on glucosidase activities. *Pharmaceuticals (Basel)*. 2019;12(3):108.
47. a) Mykhailiuk PK. Saturated bioisosteres of benzene: where to go next? *Org Biomol Chem*. 2019;17(11):2839–2849. b) Measom ND, Down KD, Hirst DJ, Jamieson C, Manas ES, Patel VK, Somers DO. Investigation of a bicyclo[1.1.1]pentane as a phenyl replacement within an LpPLA<sub>2</sub> inhibitor. *ACS Med Chem Lett*. 2017;8(1):43–48. c) Stepan AF, Subramanyam C, Efremov IV, Dutra JK, O’Sullivan TJ, DiRico KJ, McDonald WS, Won A, Dorff PH, Nolan CE, et al. Application of the bicyclo[1.1.1]pentane motif as a nonclassical phenyl ring bioisostere in the design of a potent and orally active  $\gamma$ -secretase inhibitor. *J Med Chem*. 2012;55(7):3414–3424.
48. Rowland RJ, Wu L, Davies GJ. 6BK Crystal structure of human alpha-galactosidase A in complex with alpha-galactose configured cyclosulfamidate ME763. *Rcsb Pdb*. 2019.
49. a) Hill CH, Viuff AH, Spratley SJ, Salamone S, Christensen SH, Read RJ, Moriarty NW, Jensen HH, Deane JE. Azasugar inhibitors as pharmacological chaperones for Krabbe disease. *Chem Sci*. 2015;6(5):3075–3086. b) Won J-S, Singh AK, Singh I. Biochemical, cell biological, pathological, and therapeutic aspects of Krabbe’s disease. *J Neurosci Res*. 2016;94(11):990–1006.
50. Ayers BJ, Ngo N, Jenkinson SF, Martínez RF, Shimada Y, Adachi I, Weymouth-Wilson AC, Kato A, Fleet GWJ. Glycosidase inhibition by all 10 stereoisomeric 2,5-dideoxy-2,5-imino-hexitols prepared from the enantiomers of glucuronolactone. *J Org Chem*. 2012;77(18):7777–7792.
51. Kato A, Yamashita Y, Nakagawa S, Koike Y, Adachi I, Hollinshead J, Nash RJ, Ikeda K, Asano N. 2,5-Dideoxy-2,5-imino-d-altritol as a new class of pharmacological chaperone for Fabry disease. *Bioorg Med Chem*. 2010;18(11):3790–3794.
52. Sobala ŁF, Fernandes PZ, Hakki Z, Thompson AJ, Howe JD, Hill M, Zitzmann N, Davies S, Stamatakis Z, Butters TD, et al. Structure of human endo- $\alpha$ -1,2-mannosidase (MANEA), an antiviral host-glycosylation target. *Proc Natl Acad Sci USA*. 2020;117(47):29595–29601.
53. Uhlén M, Fagerberg L, Hallström BM, Lindskog C, Oksvold P, Mardinoglu A, Sivertsson Å, Kampf C, Sjöstedt E, Asplund A, et al. Tissue-based map of the human proteome. *Science*. 2015;347(6220):1260419.

54. Hamilton SR, Li H, Wischnewski H, Prasad A, Kerley-Hamilton JS, Mitchell T, Walling AJ, Davidson RC, Wildt S, Gerngross TU, et al. Intact  $\alpha$ -1,2-endomannosidase is a typical type II membrane protein. *Glycobiology*. 2005;15(6):615–624.
55. Koyama R, Kano Y, Kikushima K, Mizutani A, Soeda Y, Miura K, Hirano T, Nishio T, Hakamata W. A novel Golgi mannosidase inhibitor: molecular design, synthesis, enzyme inhibition, and inhibition of spheroid formation. *Bioorg Med Chem*. 2020;28(11):115492.
56. a) Clemons M, Danson S, Howell A. Tamoxifen ('Nolvadex'): a review. *Cancer Treat Rev*. 2002;28(4):165–180. b) Heel RC, Brogden RN, Speight TM, Avery GS. Tamoxifen: a review of its pharmacological properties and therapeutic use in the treatment of breast cancer. *Drugs*. 1978;16(1):1–24. c) Botti V, Menzel O, Staedler D. A state-of-the-art review of tamoxifen as a potential therapeutic for Duchenne muscular dystrophy. *Front Pharmacol*. 2022;13:1030785.
57. Koyama R, Hakamata W, Hirano T, Nishio T. Identification of small-molecule inhibitors of human Golgi mannosidase via a drug repositioning screen. *Chem Pharm Bull (Tokyo)*. 2018;66(6):678–681.
58. a) Wang J, Zhao Y, Zhao W, Wang P, Li J. Total synthesis of *N*-butyl-1-deoxynojirimycin. *J Carbohydr Chem*. 2016;35(8-9):445–454. b) Schäfer W, Helferich B.  $\alpha$ -Methyl d-glucoside. *Org Synth*. 1941;1:364–366. c) Li CW, Dong HJ, Cui CB. The synthesis and antitumor activity of twelve galloyl glucosides. *Molecules*. 2015;20(2):2034–2060. d) Fernández-Herrera MA, Mohan S, López-Muñoz H, Hernández-Vázquez JMV, Pérez-Cervantes E, Escobar-Sánchez ML, Sánchez-Sánchez L, Regla I, Pinto BM, Sandoval-Ramírez J, et al. Synthesis of the steroidal glycoside (25R)-3 $\beta$ ,16 $\beta$ -diacetoxo-12,22-dioxo-5 $\alpha$ -cholestan-26-yl  $\beta$ -D-glucopyranoside and its anti-cancer properties on cervicouterine HeLa, CaSki, and ViBo cells. *Eur J Med Chem*. 2010;45(11):4827–4837. e) Koppolu SR, Niddana R, Balamurugan R. Gold-catalysed glycosylation reaction using an easily accessible leaving group. *Org Biomol Chem*. 2015;13(18):5094–5097. f) Ma Y, Liu S, Xi Y, Li H, Yang K, Cheng Z, Wang W, Zhang Y. Highly stereoselective synthesis of aryl/heteroaryl- C-nucleosides *via* the merger of photoredox and nickel catalysis. *Chem Commun (Camb)*. 2019;55(97):14657–14660. g) Compain P, Decroocq C, Iehl J, Holler M, Hazelard D, Mena Barragán T, Ortiz Mellet C, Nierengarten J-F. Glycosidase inhibition with fullerene iminosugar balls: a dramatic multivalent effect. *Angew Chem Int Ed*. 2010;49(33):5753–5756.
59. a) Marjanovic Trajkovic J, Milanovic V, Ferjancic Z, Saicic RN. On the asymmetric induction in proline-catalyzed aldol reactions: reagent-controlled addition reactions of 2,2-dimethyl-1,3-dioxane-5-one to acyclic chiral  $\alpha$ -branched aldehydes. *Eur J Org Chem*. 2017;2017(41):6146–6153. b) Ferjancic Z, Saicic RN. Combining organocatalyzed aldolization and reductive amination: an efficient reaction sequence for the synthesis of iminosugars. *Eur J Org Chem*. 2021;2021(22):3241–3250.
60. Marjanovic J, Ferjancic Z, Saicic RN. Organocatalyzed synthesis of (–)-4-epi-fagomine and the corresponding pipercolic acids. *Tetrahedron*. 2015;71(38):6784–6789.
61. Trajkovic JM, Ferjancic Z, Saicic RN. A short stereoselective synthesis of (+)-aza-galacto-fagomine (AGF). *Tetrahedron*. 2017;73(18):2629–2632.
62. Carabateas PM, Surrey AR, Harris LS. and Antitussive activity of a new heterocyclic ring system. some 1,2-diazabicyclo[2.2.2]octanes. *J Med Chem*. 1964;7(3):293–297.
63. a) Trajkovic M, Balanac V, Ferjancic Z, Saicic RN. Total synthesis of (+)-swainsonine and (+)-8-epi-swainsonine. *RSC Adv*. 2014;4(96):53722–53724. b) Trajkovic M, Pavlovic M, Bihelovic F. Total synthesis of (+)-swainsonine, (–)-swainsonine, (+)-8-epi-swainsonine and (+)-dideoxy-imino-lyxitol by an organocatalyzed aldolization/reductive amination sequence. *Nat Prod Commun*. 2022;17(4):1934578X2210916.
64. a) Cao Y, Yang R, Lee I, Zhang W, Sun J, Wang W, Meng X. Characterization of the SARS-CoV-2 E protein: sequence, structure, viroporin, and inhibitors. *Protein Sci*. 2021;30(6):1114–1130. . b) Wang K, Xie S, Sun B. Viral proteins function as ion channels. *Biochim Biophys Acta*. 2011;1808(2):510–515. c) See Ref. 28 and in particular Ref. 28b, in which the authors contest the correlation of the inhibitory activity of DNJ on ER  $\alpha$ -glucosidases with its anti-BVDV activity. [33813796]
65. a) Chang AY, Chau V, Landas JA, et al. Preparation of calcium competent *Escherichia coli* and heat-shock transformation. *JEMI Methods*. 2017;1:22–25. b) Yamamoto K, Nakayama A, Yamamoto Y, Tabata S. Val216 decides the substrate specificity of  $\alpha$ -glucosidase in *Saccharomyces cerevisiae*. *Eur J Biochem*. 2004;271(16):3414–3420.
66. Trombetta ES, Simons JF, Helenius A. Endoplasmic reticulum glucosidase II is composed of a catalytic subunit, conserved from yeast to mammals, and a tightly bound noncatalytic HDEL-containing subunit. *J Biol Chem*. 1996;271(44):27509–27516.
67. a) Prodanović R, Milosavić N, Jovanović S, Prodanović O, Ćirković Veličković T, Vujčić Z, Jankov RM. Activity and stability of soluble and immobilized  $\alpha$ -glucosidase from baker's yeast in cosolvent systems. *Biocatal Biotransform*. 2006;24(3):195–200. b) <https://www.graphpad.com/quickcalcs/linear1/>. (last accessed 10 March 2023).c) Guce AI, Clark NE, Salgado EN, Ivanen DR, Kulminkaya AA, Brumer H, Garman SC. Catalytic mechanism of human  $\alpha$ -galactosidase. *J Biol Chem*. 2010;285(6):3625–3632.
68. Ichikawa Y, Igarashi Y, Ichikawa M, Suhara Y. 1-*N*-Iminosugars: potent and selective inhibitors of  $\beta$ -glycosidases. *J Am Chem Soc*. 1998;120(13):3007–3018.
69. Bhuma N, Burade SS, Louat T, Herman J, Kawade S, Doshi PJ, Dhavale DD. Fluorinated piperidine iminosugars and their *N*-alkylated derivatives: synthesis, conformational analysis, immunosuppressive and glycosidase inhibitory activity studies. *Tetrahedron*. 2018;74(8):852–858.
70. a) Li Y, Liu D, Wang Y, Su W, Liu G, Dong W. The importance of glycans of viral and host proteins in enveloped virus infection. *Front Immunol*. 2021;12:638573. b) Jan J-T, Cheng T-JR, Juang Y-P, et al. Identification of existing pharmaceuticals and herbal medicines as inhibitors of SARS-CoV-2 infection. *Proc Natl Acad Sci USA*. 2021;118(5):e2021579118.
71. Nunes-Santos CJ, Kuehn HS, Rosenzweig SD. N-glycan modification in COVID-19 pathophysiology: in vitro structural changes with limited functional effects. *J Clin Immunol*. 2021;41(2):335–344.
72. Guo, et al. reported that miglustat inhibits the entry of SARS-CoV into a host cell via a post-receptor-binding mechanism. See Ref.16.
73. Rajasekharan S, Milan Bonotto R, Nascimento Alves L, Kazungu Y, Poggianella M, Martinez-Orellana P, Skoko N, Polez S, Marcello A. Inhibitors of protein glycosylation are active against the coronavirus severe acute respiratory syndrome coronavirus SARS-CoV-2. *Viruses*. 2021;13(5):808.

74. a) Hoffmann M, Mösbauer K, Hofmann-Winkler H, Kaul A, Kleine-Weber H, Krüger N, Gassen NC, Müller MA, Drosten C, Pöhlmann S, et al. Chloroquine does not inhibit infection of human lung cells with SARS-CoV-2. *Nature*. 2020;585(7826):588–590. b) Funnell SGP, Dowling WE, Muñoz-Fontela C, Gsell P-S, Ingber DE, Hamilton GA, Delang L, Rocha-Pereira J, Kaptein S, Dallmeier KH, et al. Emerging preclinical evidence does not support broad use of hydroxychloroquine in COVID-19 patients. *Nat Commun*. 2020;11(1):4253. c) Maisonnasse P, Guedj J, Contreras V, et al. Hydroxychloroquine use against SARS-CoV-2 infection in non-human primates. *Nature*. 2020;585:584–587.
75. Clarke EC, Nofchissey RA, Ye C, Bradfute SB. The iminosugars celgosivir, castanospermine and UV-4 inhibit SARS-CoV-2 replication. *Glycobiology*. 2021;31(4):378–384.
76. Franco EJ, Warfield KL, Brown AN. UV-4B potently inhibits replication of multiple SARS-CoV-2 strains in clinically relevant human cell lines. *Front Biosci (Landmark Ed)*. 2022;27(1):3.
77. Reyes H, Du Y, Zhou T, et al. Glucosidase inhibitors suppress SARS-CoV-2 in tissue culture and may potentiate. *bioRxiv*. 2021;2021.05.14.444190.
78. Karade SS, Franco EJ, Rojas AC, et al. Structure-based design of potent iminosugar inhibitors of endoplasmic reticulum  $\alpha$ -glucosidase I with anti-SARS-CoV-2 activity. *J Med Chem*. 2023;66(4):2744–2760.
79. Overkleeft HS, Renkema GH, Neele J, et al. Generation of specific deoxynojirimycin-type inhibitors of the non-lysosomal glucosylceramidase. *J Biol Chem*. 1998;273(41):26522–26527.
80. Zu S, Luo D, Li L, et al. Tamoxifen and clomiphene inhibit SARS-CoV-2 infection by suppressing viral entry. *Signal Transduct Target Ther*. 2021;6(1):435.
81. Principle of multivalency: a) Ramos-Soriano J, Rojo J. Glycodendritic structures as DC-SIGN binders to inhibit viral infections. *Chem Commun (Camb)*. 2021;57(42):5111–5126. b) Schneider JP, Tommasone S, Della Sala P, et al. Synthesis and glycosidase inhibition properties of calix[8]arene-based iminosugar click clusters. *Pharmaceuticals*. 2020;13(11):366. c) Illescas BM, Rojo J, Delgado R, et al. Multivalent glycosylated nanostructures to inhibit Ebola virus infection. *J Am Chem Soc*. 2017;139(17):6018–6025.
82. a) Protein Preparation Wizard. Epik. New York (NY): Schrödinger, LLC; 2021. b) Impact. New York (NY): Schrödinger, LLC; c) Prime. New York (NY): Schrödinger, LLC; 2021. d) Madhavi Sastry G, Adzhigirey M, Day T, et al. Protein and ligand preparation: parameters, protocols, and influence on virtual screening enrichments. *J Comput Aided Mol Des*. 2013;27(3):221–234.
83. Schrödinger release 2021–4: Maestro. New York (NY): Schrödinger, LLC.
84. a) Schrödinger Release 2021-1: Epik, Schrödinger, LLC, New York, NY, 2021. b) Shelley JC, Cholleti A, Frye LL, et al. Epik: a software program for pK<sub>a</sub> prediction and protonation state generation for drug-like molecules. *J Comput Aided Mol Des*. 2007;21(12):681–691.
85. a) Schrödinger release 2021–4: Glide. New York (NY): Schrödinger, LLC; 2021. b) Friesner RA, Murphy RB, Repasky MP, Frye LL, Greenwood JR, Halgren TA, Sanschagrin PC, Mainz DT. Extra precision glide: docking and scoring incorporating a model of hydrophobic enclosure for protein-ligand complexes. *J Med Chem*. 2006; 49:6177–6196.
86. BIOVIA Discovery Studio 2021 Client. San Diego: Dassault Systèmes; 2021.
87. a) Harwood LM. Dry-column flash chromatography. *Aldrichimica Acta*. 1985;18(1):25. b) Furniss BS, Hannaford AJ, Smith PWG, et al. Dry-column flash chromatography. *Vogel's Textbook of Practical Organic Chemistry*. 5th ed. London: Longman Scientific & Technical; 1989. p. 220.c) Pedersen D, Rosenbohm C. Dry column vacuum chromatography. *Synthesis (Stuttg)*. 2004; 2001(16):2431–2434.
88. Perrin DD, Armarego WLF. Purification of laboratory chemicals. 3rd ed. Oxford: Pergamon Press; 1988.
89. Messner M, Kozhushkov SI, de Meijere A. Nickel- and palladium-catalyzed cross-coupling reactions at the bridgehead of bicyclo[1.1.1]pentane derivatives - a convenient access to liquid crystalline compounds containing bicyclo[1.1.1]pentane moieties. *Eur J Org Chem*. 2000;2000(7):1137–1155.
90. Caputo DFJ, Arroniz C, Dürr AB, Mousseau JJ, Stepan AF, Mansfield SJ, Anderson EA. Synthesis and applications of highly functionalized 1-halo-3-substituted bicyclo[1.1.1]pentanes. *Chem Sci*. 2018;9(23):5295–5300.
91. Wennekes T, Lang B, Leeman M, Marel G. A v d, Smits E, Weber M, Wiltenburg J. v, Wolberg M, Aerts JMFG, Overkleeft HS. Large-scale synthesis of the glucosylceramide synthase inhibitor *N*-[5-(adamantan-1-yl-methoxy)-pentyl]-1-deoxynojirimycin. *Org Process Res Dev*. 2008;12(3):414–423.
92. Wennekes T, Meijer AJ, Groen AK, Boot RG, Groener JE, van Eijk M, Ottenhoff R, Bijl N, Ghauharali K, Song H, et al. Dual-action lipophilic iminosugar improves glycemic control in obese rodents by reduction of visceral glycosphingolipids and buffering of carbohydrate assimilation. *J Med Chem*. 2010;53(2):689–698.